Title
Absorption-Enhanced Organic Photovoltaic By Incorporating Metallic Nano Pyramid Particles

Author
Qasem, Hussamaldeen S.

Publication Date
2014

Peer reviewed|Thesis/dissertation

UNIVERSITY OF CALIFORNIA

Los Angeles

On Absorption-Enhanced Organic Photovoltaic By Incorporating Metallic Nano Pyramid Particles

A Thesis submitted in partial satisfaction

of the requirements for the degree Master of Science

in Electrical Engineering

by

Hussamaldeen Saif Qasem

2014

ABSTRACT OF THE THESIS

On Absorption-Enhanced Organic Photovoltaic By Incorporating Metallic Nano Pyramid Particles

by

Hussamaldeen S. Qasem

Master of Science in Electrical Engineering

University of California, Los Angeles, 2014

Professor Kang L. Wang, Chair

A lattice structure of metallic Nano pyramids (NPY) particles was planted on the interface between hole transport layer (HTL) and the transparent conductive layer (TCL) of an organic photovoltaic (OPV) cell. Standard metal evaporation along with Nano sphere lithography was used to grow the metallic NPY mesh structure. Silver (Ag) and Gold (Au) were the primary choice of the NPY mesh structure due to the excellent overlap of their peak localized surface Plasmon resonance (LSPR) frequency with the active layer absorption wavelengths. The current-voltage curve displayed an improvement in the efficiency and fill factor values of OPVs that used NPY lattice structure over devices that used regular sphere-shaped Nano particles. Despite the better-shaped and strong (LSPR) peak frequency of the Ag NPY lattice structure, Au NPY lattice structure exhibited an enhanced absorption and overall efficiency, which was owed to the wider (LSPR) frequency peak that Au possesses. The effect of NPY lattice structure could be further investigated with several approaches such as using different NPY materials, using core-shill approach, and growing the NPY on different layers or interfaces.

The thesis of Hussamaldeen Saif Qasem is approved.

Diana L. Huffaker

Dwight C. Streit

Kang L. Wang, Committee Chair

University of California, Los Angeles

2014

Table of Contents

List of Figures

1. Introduction

Organic Photovoltaic (OPV) is a photoelectric conversion device that is created from semi-conductive carbon-based materials. Depending on the OPV device type, employed organic semiconductors can take the form of conjugated polymers, dye and pigment monomers, or liquid crystals. As a principle type of OPVs, polymer solar cells deploy a blend of an acceptor type of conductive polymers and a donor type of "0D" Carbon allotrope derivatives (fullerenes). Schematic diagram of a typical organic solar cell device is presented in figure 1. The hefty advantages that plastic solar cell can bring made it a hot research topic in the last decade and a half. In contrast to inorganic semiconductor solar cell, OPVs can be produced with dramatic inexpensive, environmentally friendly, carbon-based materials with low temperature processes [1]. Moreover, their flexibility, transparency, and their lightweight nature make them monumentally convenient for reel-to-reel high-speed manufacturing. Additionally, OPV's high absorption coefficient along with their efficient indoor performance provides it with a great potential of integration with portable electronic devices [2]. Figure 2 presents a number of OPV applications.

1.1 Background

For many years, organic polymers were not believed to be having conductors properties; in fact organic polymers were widely used for insolation purposes. In early seventies, research groups started to mix carbon-based polymers with metals to form conducting composites, which showed minor conductivity enhancement. It was not until 1977, when polyacetylene (figure 3), a low conductivity polymer, exhibited a 10 order of magnitude enhancement of conductivity after reacting with Iodine [3]. As a result of this study, Hideki Shirakawa, Alan G. MacDiarmid and Alan J. Heeger have become Nobel laureates in Chemistry in the year 2000.

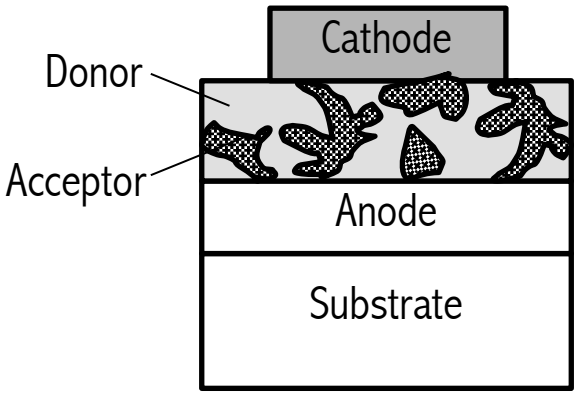

Figure 1.1.1. Typical OPV constituted of a transparent conductive layer (anode) coated on a glass substrate. Photo absorption layer is spin coated on the anode and realized by blending conjugated polymers. Thin layer of metal is deposited on the active layer as a Cathode.

The conductivity enhancement of conjugated polymer solar cells is the result of higher mobility unrestrained electron formed due to the hybridization of s and p orbitals of the conjugated polymer [4]. The electronic configuration of a ground state carbon atom is in the form of $1s^2 2s^2 2p_x^1 2p_y^1$, and after hybridization they translate into three σ sp^2 and one overlapping p_z which has a π bond that provide that unrestrained high mobility electron. Hence, giving the carbon-based material the semiconductive properties. The first realizable solar cell out of these conjugated polymers was in 1983 with a tenuous power conversion efficiency (PCE) of 0.01% [5]. In 1992, the deployment of the newly then discovered spherical fullerene molecule (C_{60}. Figure 3) with conductive polymers have mirrored inorganic semiconductors in terms of photo induced electron transport [6]. Consequently, the same research group has published a study a year later that used the conductive polymer- fullerene structure to realize multiple solid-state devices such as diodes, photodiodes, and photovoltaic devices [7].

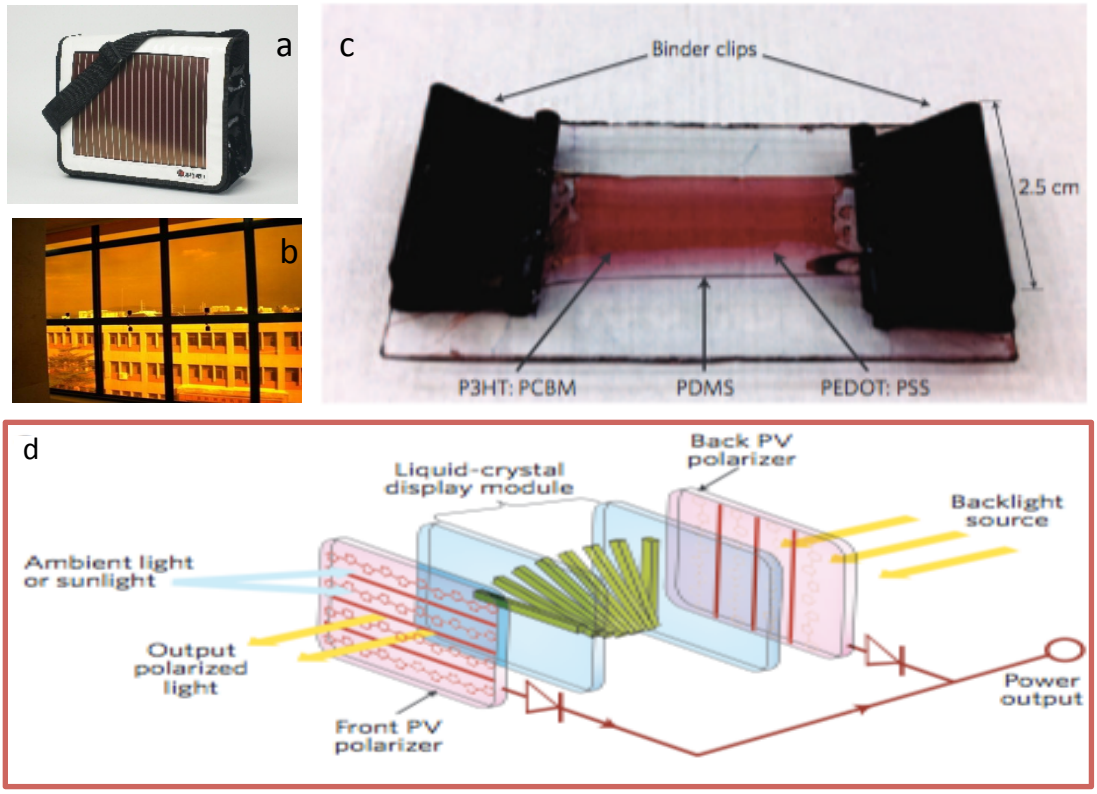

Figure 1.1.2. a-b) OPV integrated bag and window. c) Elongated OPV cell resembles flexibility [2]. d) Integrating OPV into liquid crystal display unit (LCD) [2].

Three years, the concept of blending the polymer and fullerene to overcome the low diffusion length of the photo-induced carriers, and to maximize the acceptor-donor junction area was presented [8]. Since then, polymer solar cells have passed through a golden decade, starting from less than 1% on late 1990, passing through a couple of efficiency boost on 2006 (3-4%) and on 2009 (5%) with the invention of newly polymer-fullerene blends of (P3HT- $PC_{60}BM$, figure 3) [9] and (PCDTBT-$PC_{71}BM$, figure 3) [10] respectively, and ending up with an approximately 8% efficiency on 2011 after conceiving a single layer, narrow bandgap OPV system (PTB7-$PC_{71}BM$, figure 3), which significantly decreased charge recombination, and hence, an increase in the PCE [11].

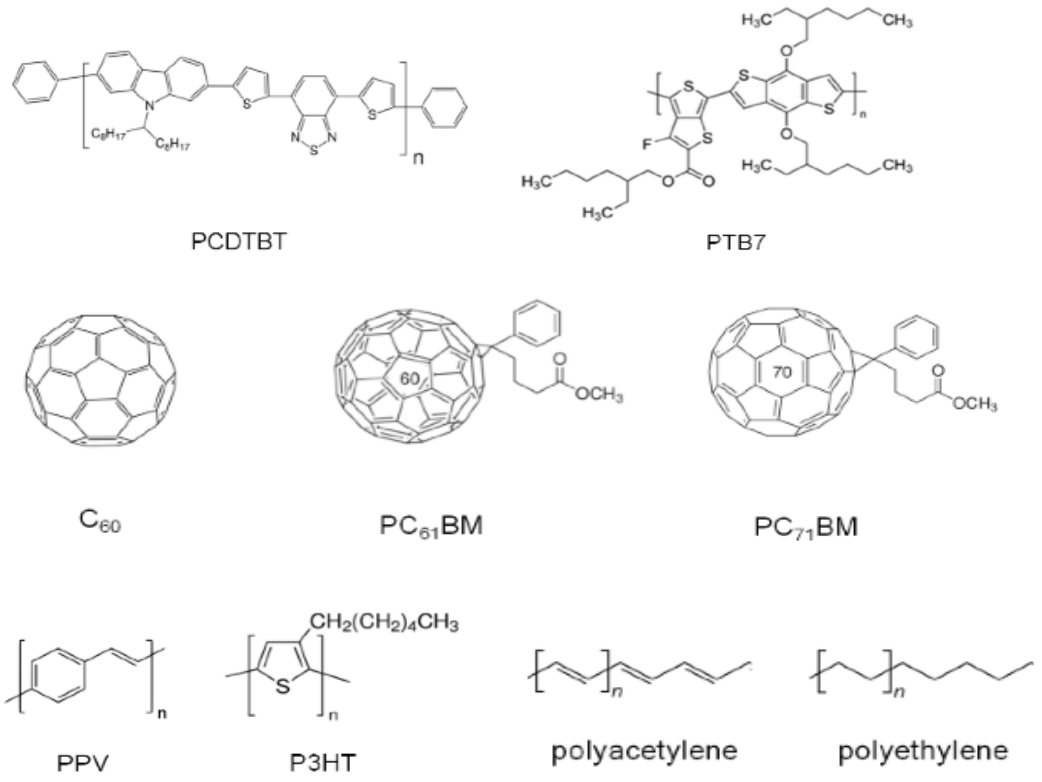

Figure 1.1.3. Different conjugated polymers and fullerene derivatives that are applied to polymer solar cells.

On a yearly basis, the National Renewable Energy Lab (NREL) publish a chart the presents the latest record efficiencies of photovoltaic cells that are being spotlighted by the research community [12]. In the chart, the notable PCE records of UCLA and its sister campus UCSB in OPV and dye-sensitized solar cells (DSSC) respectively are praiseworthy. The 2014 NREL world record efficiency chart is presented on figure 5.

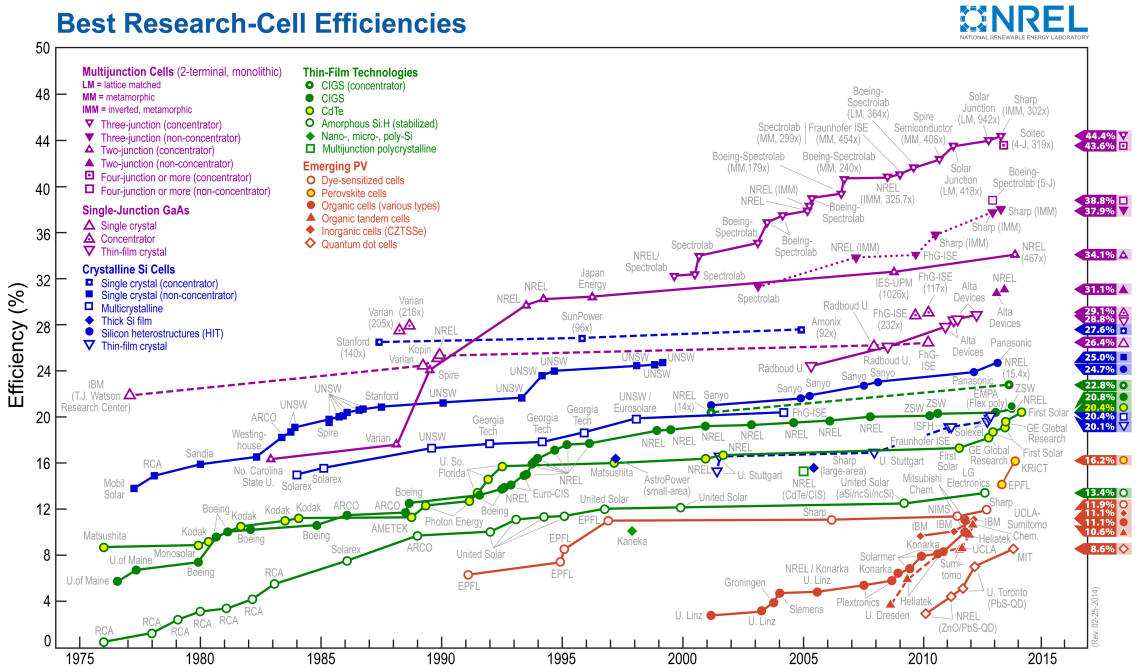

Figure 1.1.4. Best research solar cell efficiencies reported by NREL (© 2014 NREL).

1.2 Motivation

With the abundance of solar resources that exist globally (figure 1.2.2), and the considerable reduction in silicon-based solar cell prices, the idea of adapting solar cells as an energy source becomes more sensible (figure 1.2.1).

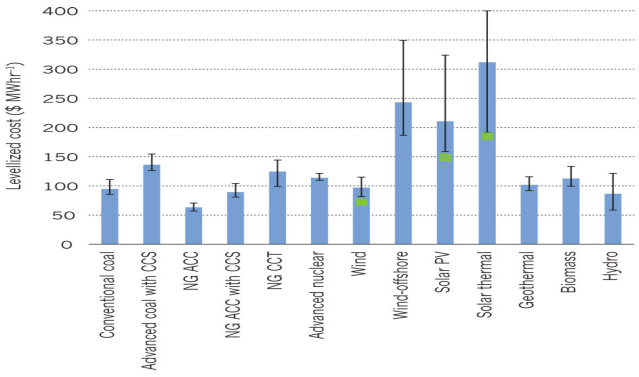

Figure 1.2.1. Projection by the US EIA made in 2010 of the 2016 average cost. Note that PV's Prices have witnessed a great reduction, it is already lower (in 2012) than the projection prices of (2016) [13].

An interesting fact about the scalability of the solar energy that is well known among solar cell technologist and scientists is that the energy that hit the earth surface per unit time is enough to provide the world with almost X10000 times the energy that it actually need per unit time (figure 1.2.2). However, the global fossil fuel energy prices have made the competition backbreaking for solar cells. The need to push down photovoltaic cost, and to provide governmental incentives is vital to survive and prevail [13, 14].

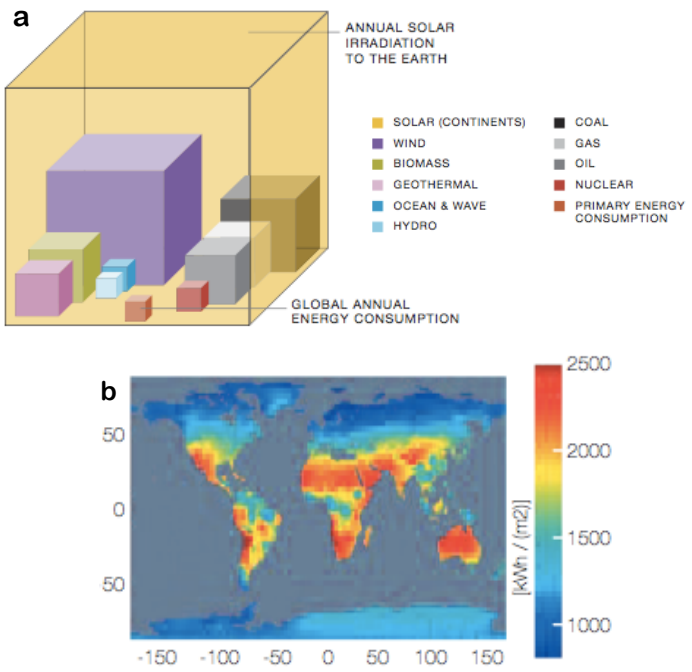

Figure 1.2.2. a) Solar irradiation versus established global energy resources, b) Solar radiation around the world [14].

In this work, and in parallel to virtually all-photovoltaic research, we tried to pursue an enhanced overall efficiency in a cheapened cost cell. The idea of this work was to incorporate special shaped metallic Nano particles in OPVs to increase the absorption, henceforth, increasing the efficiency (figure 1.2.3)

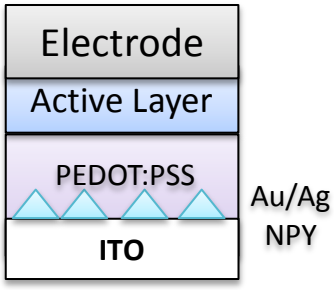

Figure 1.2.3. Layer by layer schematic of polymer solar cell with metallic Nano pyramids grown on the ITO/Buffer layer interface.

1.3 Thesis Outline

Chapter 2 starts with an introduction on photovoltaic in terms of theory, working principle, measurement parameters, and different electronic properties in sections 2.1 and 2.2. The next section, 2.3, will discuss the science of organic photovoltaic and the contrast between organic and inorganic photovoltaic in terms of the device physics. Section 2.4 includes an introduction and compact details about localized surface Plasmon resonance (LSPR) and it's relation to the absorption enhancement.

Chapter 3 will present and examine the experimental data acquired from measurements implemented on our NPY-enhanced OPV devices. The chapter starts with a short run-through of the research implemented on NPY-enhanced OPV until now, and followed by detailed, layer-by-layer fabrication techniques of our device. Measurement results that analyze size dependence, geometrical shape dependence, material dependence, and intra space between particle dependence are displayed and discussed in sections 3.2. Section 3.3 provides a presentation of new electron conducting layer material that is employed to enhance both the charge-transport and charge-collection efficiencies. Optimization of the new materials thicknesses and solvent

concentration are displayed on the same section. The tail of the chapter will discuss encapsulation techniques, packaging techniques, and durability study of our device (3.4).

Chapter 4 provides will give a panoramic and concise view of the advantages, and challenges that face the OPV device in the case of depositing the NPY particles in the electrode/active layer interface (opposite side).

An all-in-all conclusion of the thesis and an overview of the OPV's research future statues forecasting are presented in chapter 5.

2. Working Principle and Electronic Properties of Organic Photovoltaic

The basic phenomenon behind the photovoltaic effect, the production of electric current after light exposure, is the photoelectric effect. In 1905, and in one of his Annus mirabilis four papers, A. Einstein proposed and experimentally proved the photoelectric effect [15]. In part, the phenomenon states that adequate energetic photons can liberate electrons bounded to solids. These liberated electrons can be exploited in a circuit to produce power, hence, a photovoltaic device. The first photovoltaic device was put together long before the discovery of the photoelectric effect, when A. Becquerel shined light into a piece of Silver Chloride that was submerged in an acidic liquid, he found that a connected ammeter could pick up current [16]. Schematic of both photoelectric and photovoltaic effect is presented in the bottom of this page.

2.1 Photovoltaic Physics and Parameters

The simplest model of a PV device is the pn junction, which is an interface between a p type and an n type semiconductor. Doping, which is replacing a number of the material's atoms with another material's atom, is what gives the semiconductor the p or n label. When a material of group IV in the periodic table is doped with a material from group V, the produced n doped semiconductor will have extra electrons or as sometimes called charge carriers.

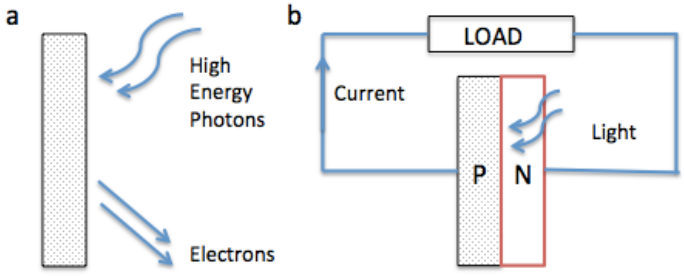

Figure 2.1.1. Schematic of both a) photoelectric and b)photovoltaic effect.

On the contrary, doping the semiconductor with group III material will product into a p type semiconductor that lacks an electron, the lack of an electron is dealt with as a particle in quantum mechanics, this particle is called a hole, holes also can be categorized as charge carriers. Deeper explanation is presented in Singh [17], however, for our device it serves enough to state that when a p doped semiconductor and an n doped semiconductor are brought together, the dopant atoms preserve their locations, and their extra charge carriers diffuse through the junction line. An internal electric field will be built across the boundary, which will deplete any charge carrier that is produced near that boundary in the reverse direction (figure 2.1.2 a-b). The built in electric field will in turn cause the charge carriers to flow, forming the electric current; hence, a very basic form of solar cell is created [17].

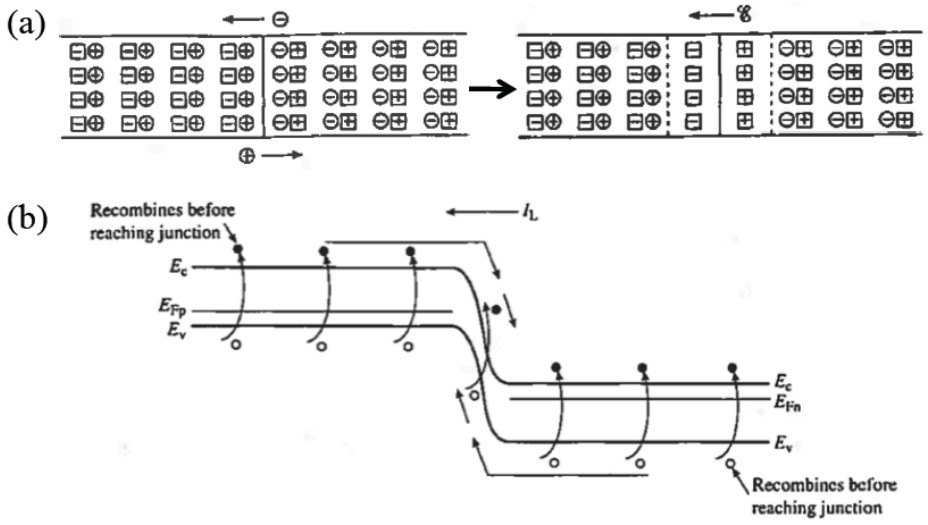

Figure 2.1.2. a) Charge carriers diffuse across the junction upon pn junction formation, the traveled charge carriers will leave an immobile ions (squares). Which will result in an internal electric field to balance the diffusion potential. b) pn junction der illumination, excited carriers close to the junction will have the ability to jump and create energy in the external circuit, however, far carriers will recombine and fail to diffuse all the way [18].

The relation of the built in electric field versus the produced current flow shapes up the current-voltage (IV) characterization curve. As (figure 2.1.3) demonstrate, the larger the charge excitation rate, the larger the area under the curve (power) turns out to be [18].

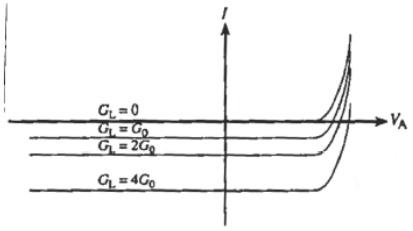

Figure 2.1.3. IV Characterization curve under different light intensities [18].

The out power is the area under the IV curve, and it can be calculated by integrating the curve. Since the curve is nearly a rectangle, we can simply multiply the open circuit voltage (highest voltage value on the v axis) by the short circuit current (highest current value on the I axis) to obtain the Power output:

$$P_{ideal} = V_{oc} \times I_{SC}$$

And since we are dealing with photovoltaic devices, and these devises comes with deferent area, the need to normalize the current value over the photovoltaic device area becomes central, hence, from now on, we will used the symbol of current density (J) instead of I, the equation will become:

$$P_{ideal} = V_{oc} \times J_{SC}$$

Nearly, no real photovoltaic device will result into a perfect rectangle shape. As figure 2.1.4 presents, the device will operate in a maximum voltage that is less than the open-circuit voltage, and will also operate in a maximum current density point that is less than the short circuit

current. Therefore, the maximum power output is actually less than the previous equation, which can be update as follow:

$$P_{max} = V_{max} \times J_{max}$$

The concept of fill factor (FF) was developed to measure how much did the photovoltaic device filled the perfect rectangle representation (as presented in figure 2.1.4), the equation is as simple as the following:

$$FF = \frac{Maximum\ Output\ Power}{Ideal\ Output\ Power} = \frac{P_{max}}{P_{ideal}} = \frac{V_{max} \times J_{max}}{V_{oc} \times J_{SC}}$$

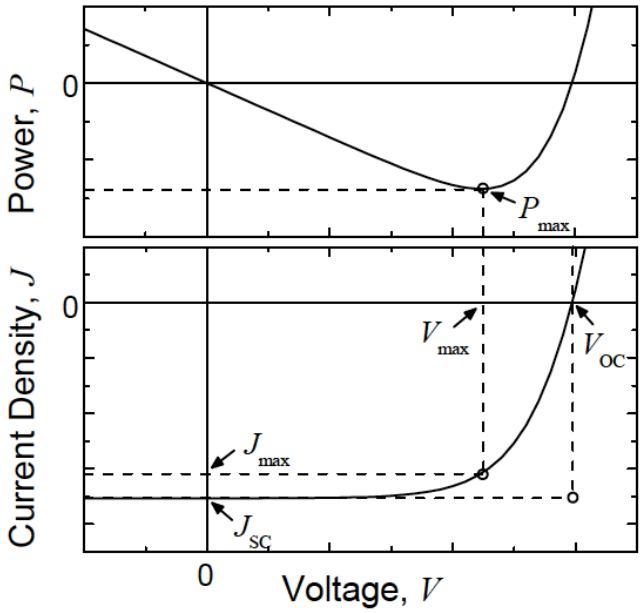

Figure 2.1.4. Photovoltaic device parameters ($V_{oc}, J_{sc}, V_{max}, and\ J_{max}$), and the correspondent instantaneous power.

The power conversion efficiency (PCE), mostly referred to as the "*efficiency*", is the primary index that characterizes a photovoltaic device, which measure the amount of the produced electrical power over the solar irradiance power shined over the cell. The irradiance should be normalized over the area, temperature and the location since the solar spectrum (solar irradiance

reaching earth surface) vary liberally depending on these factors. By convention, and unless mentioned otherwise, the standard test condition, which will produce 1000 W/m^2, is under a temperature of 25°C, an radiance area of 1m^2, and an air mass of 1.5 AM, equation becomes:

$$PCE_{Standard\ Test\ Condition} = \frac{P_{max}}{1000w/m^2}$$

Solar energy that is incident on the earth surface have a wide range of wavelengths versus a wide range of photon densities, this relation produce the famous "Solar Spectrum" graph. As mentioned in the previous paragraph, the solar spectrum is primarily a function of air mass (figure 2.1.5).

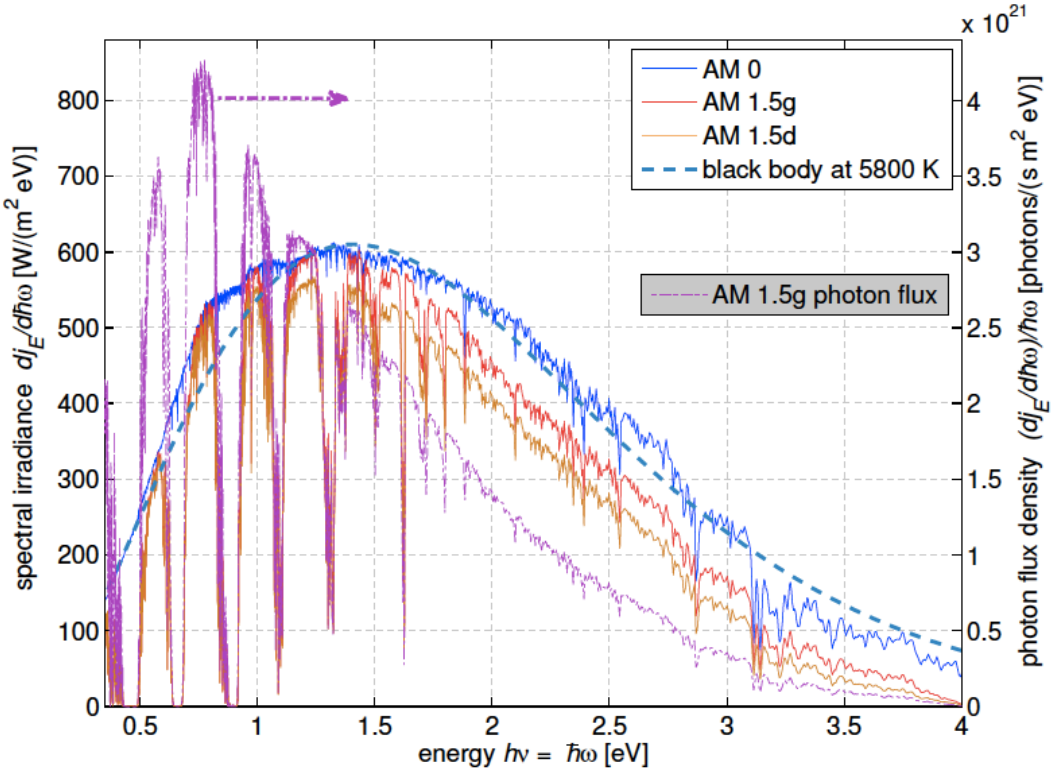

Figure 2.1.5. Solar spectrums at 1.5 Air Mass (STC), and an extra-terrestrial solar spectrum at 0 Air Mass (Black Body spectrum) [19].

Air mass is defined as the ratio between the optical path length from the sun to the optical length if the sun is perfectly overhead [20] (figure 2.1.6):

$$air\ mass = \frac{Optical\ path\ length\ from\ the\ sun}{Optical\ path\ length\ if\ the\ sun\ is\ overhead} = \frac{d_{atm}}{d_{atm-overhead}} = m\csc\gamma_s$$

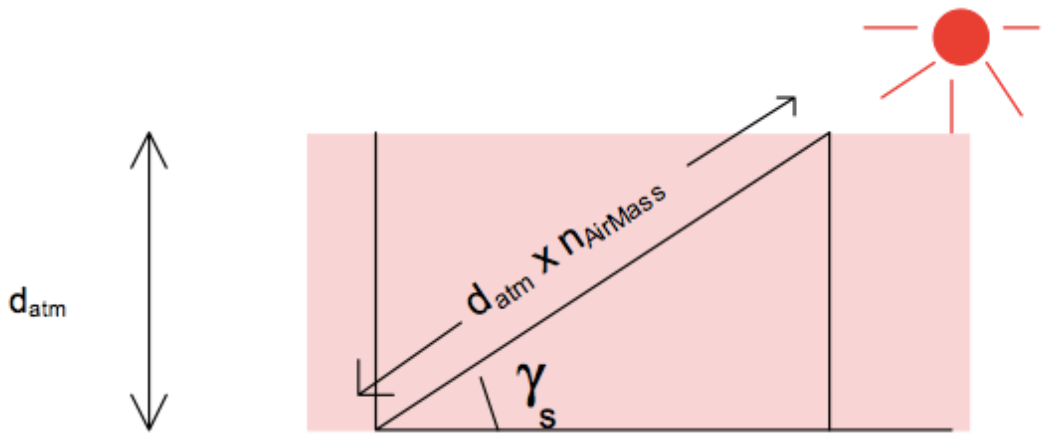

Figure 2.1.6. Photovoltaic device parameters ($V_{oc}, J_{sc}, V_{max}, and\ J_{max}$), and the correspondent instantaneous power [20].

In quantum mechanics point of view, the power conversion efficiency (PCE) is somewhat a broad parameter; therefore, the quantum efficiency (QE) has been proposed as metric that describes the photovoltaic mechanism in a great sense of accuracy. The quantum efficiency is basically the amount of charge carriers collected by the electrodes over the amount of incident photons. QE comprises of three sub-efficiencies that describes the three stages for the photon to be successfully converted into a charge carrier and delivered to the external circuit, theses sub efficiencies are absorption efficiency, charge separation efficiency, charge collection efficiency.

$$QE = \frac{No.of\ incident\ photons\ no\ the\ cell}{No.of\ charge\ carriers\ going\ into\ the\ external\ circuit} = \eta_{abs}\eta_{CS}\eta_{CC}$$

As an initial step for the photovoltaic process, incident photon must be absorbed. However, the incident photons arrive in different wavelength, therefore, different energies. The absorption process will take place only if the photon energy is equal or larger than the material band gap, lesser energy photons will go through the materials unabsorbed, hence, an absorption efficiency will take place. Most inorganic photovoltaic have a band gap around 1 eV, which will result into a 75% absorption efficiency [20], however, OPV semiconductive polymers have a higher bandgap, hence, lower absorption efficiency (around 30%). The OPV working principles will be emphasized more in the next section.

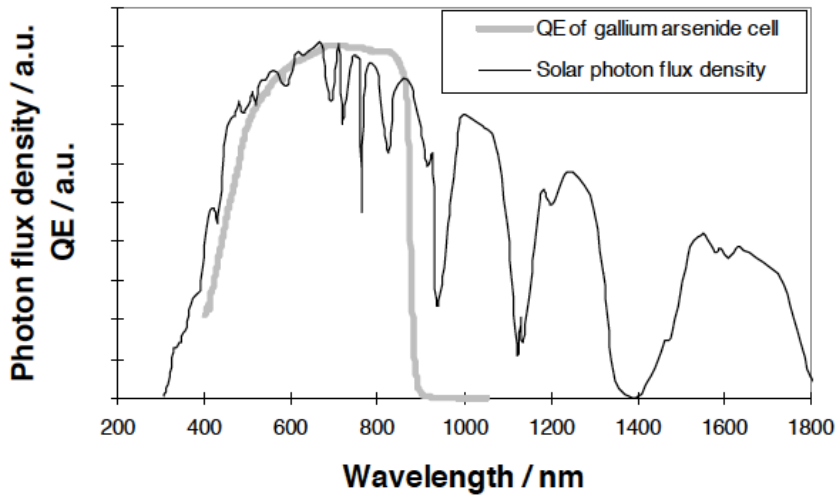

Figure 2.1.7. Relation between the quantum efficiency of GaAs and the solar spectrum, it is desirable to have a quantum efficiency that overlap with wavelength of solar spectrum that have high photon flux density [20].

If the incident photon has been absorbed then a charge carrier (e.g. electron) will be liberated and excited into the conduction band and will be forwarded to the contacts. The tow main mechanisms of transport of generated charges are drift and diffusion. The charge flow under electric field is described as drift and equated as following:

$$v = \mu E$$

Where ν is the drift velocity, μ is the mobility of charge carriers, and E is the electric field. Consequently, the overall motion of the charge carriers is called the drift current J_{Drift} and is characterize as:

$$J_{Drift} = q\mu\rho(x)E(x)$$

Where $\rho(x)$ is the charge carrier density, and q is the electron charge. Total J_{Drift} can be obtained by superpose the drift current of electrons and holes.

On the other hand, diffusion current $J_{Diffusion}$ is the result of charge motion due to charge concentration variation around the junction and characterized as the following:

$$J_{Diffusion} = qD\frac{d\rho(x)}{dx}$$

Where D is the diffusion coefficient of the charge carriers, and the later term is the flux density. It is important to understand that a number of charge carriers go back to the valence band and start a mechanism of recombination, thus, not every liberated charge carrier will be affected by diffusion or drift sufficiently to reach the electrode. The rate of the recombined charge carriers to the total number of carriers generated is responsible for the concept of charge separation efficiency and charge collection efficiency. It is relevant to this work to mention that OPVs have an extra internal quantum efficiency mechanism, which is the exciton diffusion efficiency; it will also be emphasized upon in the next section [20]. The quantum efficiency rate is related to the solar spectrum irradiance by the graph on figure 2.1.7 on the previous page.

The output short current density J_{sc} is linked to the incident photons in the following relation:

$$J_{sc} = \frac{q}{A}\int \Phi(\lambda)QE(\lambda)d\lambda$$

Where q and A is the electron electric charge and device area respectively. In the integration, there is the incoming photon flux as a wavelength dependent $\Phi(\lambda)$ and the quantum efficiency $QE(\lambda)$ that was mentioned in the previous page.

The transport of charges in solar cells undergo tow main

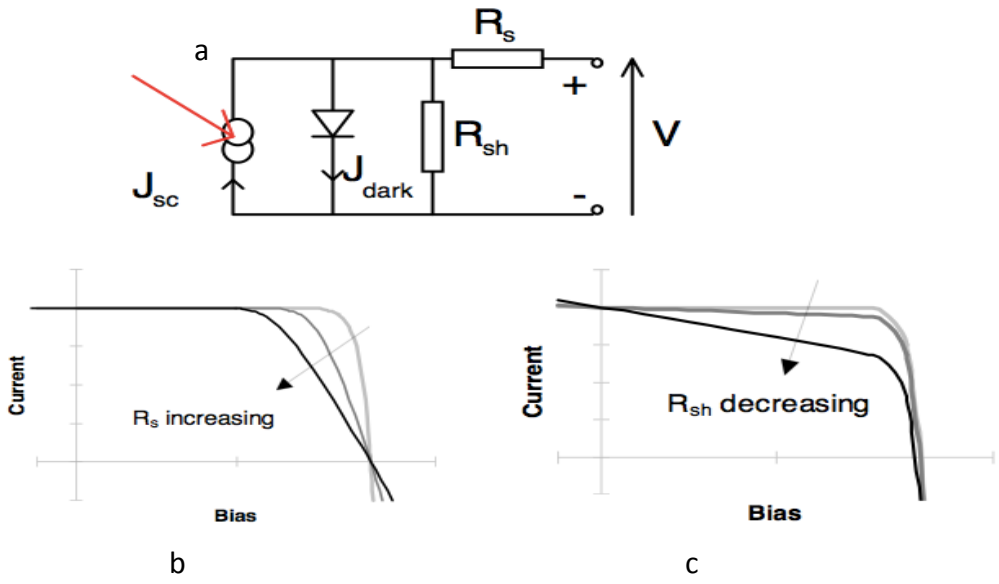

Figure 2.1.8. a) Equivalent electrical circuit of a photovoltaic. b) Effect of increasing series resistance on the power rectangle. c) Effect of decreasing the shunt resistance on the power rectangle [20]

In an electrical point of view, the equivalent circuit of an ideal solar cell is a current generator connected to a shunt non-linearly resistive element (such as a diode), a photocurrent will be produced proportional to the light intensity, however, in a real solar cell parasitic resistances will cause the current to leak and power to dissipate due to the contact resistance or the solar cell material resistance, they will be represented in the equivalent circuit as series resistance (R_s) and shunt resistance (R_{sh}). Figure 2.1.8 shows a schematic of the equivalent circuit and the effect of changing the resistance on the IV curve.

Since the basic model a photovoltaic is a pn junction, it is valid to assume that the device act as an ideal diode. Rectifying behavior will appear in the dark, and passing charges under illumination. Henceforth, deriving current and voltage equation in the same manner as we do with diodes is valid too.

The dark current density $J_{dark}(V)$ for an ideal diode is as following:

$$J_{dark}(V) = J_o(e^{\frac{qV}{KT}} - 1)$$

Where J_o is the dark saturation current or the diode leakage current in the dark, it is directly related to recombination rate, and hence, it is contrarily related to the material purity or quality. K and T is the Boltzmann's constant and the absolute temperature respectively.

It is safe to apply the superposition concept between the dark current and the short circuit current to calculate the IV characteristic current value as following:

$$J(V) = J_{dark}(V) - J_{sc}$$

Hence, the equation will be as follow:

$$J(V) = J_o\left(e^{\frac{qV}{KT}} - 1\right) - \frac{q}{A}\int \Phi(\lambda)QE(\lambda)d\lambda$$

As for the voltage equation, we can find the V_{oc} by putting $J(V)$ equation to equal 0, which will result into the following equation:

$$V_{oc} = \frac{KT}{q}\ln\left(1 + \frac{J_{sc}}{J_o}\right)$$

2.2 Organic Photovoltaic (OPV)

Unlike traditional atomic photovoltaic semi-conductive material, organic semiconductors are basically molecule-based materials. Optical properties such as absorption, and luminescence, along with electrical properties such as transport, charge carriers localization, and separation are largely affected by the molecule arrangement of the semiconductor polymers [21]. Solid-state physics point out that the presence of delocalized charges that are capable of absorbing energy from an applied field is a necessity secure electric conductivity. Organic solids are deficient in delocalized charges when compared to inorganic counterparts. Hence, much less conductivity is notable in them. However, special prepared polymers can conversely provide delocalized electrons through the π bond system [22-24]. As a famous example for polymers with delocalized electron encouraging bond arrangement, aromatic Benzene molecule offers multiple π bonds that contribute to the conductivity enhancement in the material [25]. Figure 2.2.1 feature a schematic of the hybridization concept that form the π bonds in a single molecule, in addition to, visualization of π orbitals (bonding and anti-bonding) of an Ethene and Benzene molecule. Ethene energy levels, wave functions and probability distributions graph are also displayed. According to Pauli exclusion's principle and the linear combination of atomic orbitals concept, an energy band split of the same level will take place to form a bonding band and an anti-bonding band [26]. The anti-bonding energy level is always higher than the other bonding band, and as a result of that, electron will not occupy that band before felling the bonding band [27], making it the lowest unoccupied molecular orbital (LUMO), and the filled sub band in the lower side will be the highest occupied molecular orbital (HOMO) [28]. HOMO and LUMO are analogous to the conduction band (CB) and valance band (VB) in inorganic semiconductor, thus, the energy between the HOMO and LUMO is a prohibited band, or a band gap. Moving from a

single molecular level to a group of molecules, the intra molecular bonds are principally van der Waals bonds. As for other types of intra molecular bonds, it is impossible to form due to the closed shell of each molecule, more at [29].

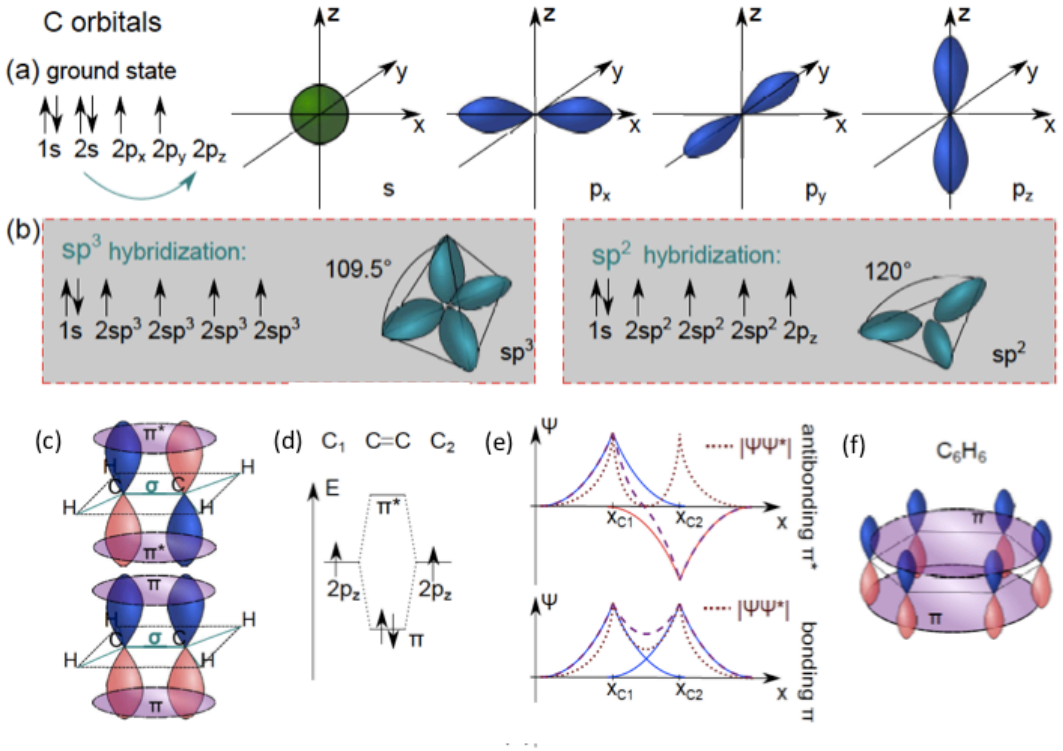

Figure 2.2.1. a) Electronic configuration of Carbon atom. b) Hybridized Carbon atom for the cases where the hybrid bonds are on the 2p sub energy level sp^3 (left), and hybrid bonds on the 2s sub energy level sp^2 (right). c) The π bonding system is generated when unhybridized perpendicular orbitals (p_z) overlap with each other, resulting in a bonding (down), and anti-bonding (up) arrangements, demonstrated molecule is Ethene. d) Ethene bonding energy levels, e) their linear combination of atomic orbitals (solid), molecular electron wave function (dashed) and probability distribution (dotted). f) Benzene molecule offers multiple numbers of π orbitals that will supply more delocalized electrons [30].

The arrangement of HOMO and LUMO in a single molecule will replicate with a small deviation if molecules are grouped to make a molecular solid, the small deviation is mainly due to the

polarizing effect. Specially prepared polymers can be put together to form a semi pn junction with an internal electric field, except that the pn junction is now called acceptor/donor junction and it can be deployed to build various types of devices such as OPV. Flat planar junction (FPJ) was firstly proposed to make an OPV device, however, low efficiencies were observed. The presence of a quasi-particle called Exciton makes it hard for OPV to acquire high quantum efficiency [31]. The nominal diffusion length for organic polymers is on the order of 10 nm, that is nearly five orders of magnitude less than silicon [32]. Bulk heterojunction polymers (BHJ) were realized in order to supply more dispersed junction contour length, hence, higher probability for exciton to be dissociated and electrons to be collected [33]. The method used to make BHJ layer is to blend both the donor material and the acceptor material in an optimized ratio. Figure 2.2.2 show the structure of both FPJ, and BHJ OPV device, in addition to the typical band diagram of OPV.

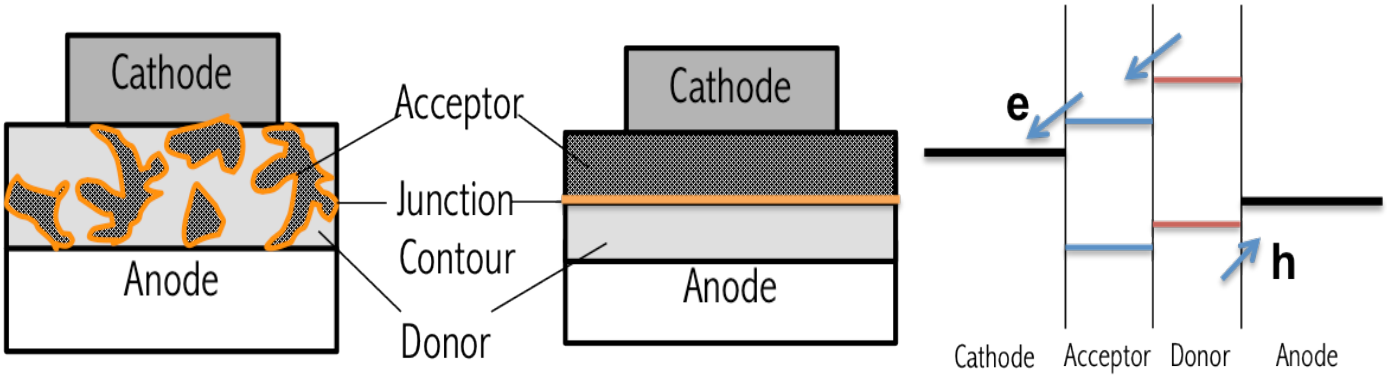

Figure 2.2.2. The structure of BHJ (left), FPJ (middle), and typical band diagram (right) of an OPV device.

On the contrary to the inorganic photovoltaic charge collection steps, OPV have one more step to make a total of four steps in order to collect a charge at the electrode. These four steps are 1) light absorption, 2) exciton generation and diffusion, 3) charge transport, and 4) charge collection. These steps will modify the quantum efficiency equation as follow:

$$QE = \eta_{abs} \times \eta_{ED} \times \eta_{CST} \times \eta_{CC}$$

- Absorption efficiency (η_{abs})

  The first step is for photon to be absorbed by the polymer materials. The majority of organic semiconductors have a high bandgap eV, which will devastate the amount and the energy of the absorbed photons. The energy of the photon have to be higher or equal to the energy of the electron bounded to the solid to be released, this is the core concept of the photoelectric effect and the previous Planck's hypothesis:

$$E = h\,\nu$$

  The bandgap of P3HT:PCBM, a famous material used regularly in OPV application, is around 1.6 eV [34], as a result, and what we expect from the absorption on graph 2.2.3 is that ultra violet and high visible wavelengths shall be absorbed, and a sharp cut off of absorption on the wavelength that corresponds to bandgap energy which is around 750 nm. The typical absorption efficiency of organic polymers is on the 30-40% regime.

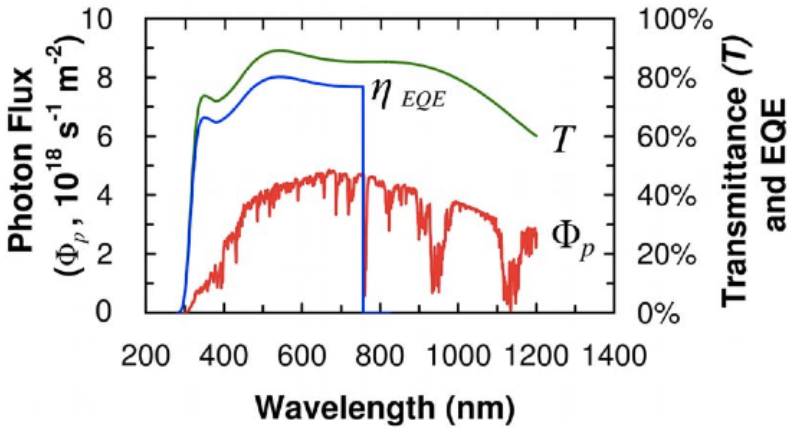

Figure 2.2.3. Absorption spectrum shows the absorption QE of P3HT:PCBM [34].

Although their might some reflection of photons on the coating surface of the OPV device, it is assumed that these losses are insignificant [35]. A great deal of research was

spent on light management category in inorganic PVs, especially on anti reflective coating. OPV can definitely benefit from those techniques.

- Exciton diffusion efficiency (η_{ED})

  An instantaneous formation of excitons takes place upon photons absorption. The exciton needs to diffuse to the donor/acceptor interface in order to be dissociated into a free electron or hole. The diffusion is very short (10 nm), hence, a drop in efficiency might take place due to exciton relaxation. However, the picture is not totally dark, high absorption coefficient of the organic polymers helps the light to be absorbed within a very thin layer [36]. We want the absorption coefficient on the least to be equal to the absorption layer thickness. The diffusion length (L_D) of excitons in OPVs was studied and modeled by Lunt et al [36] and they equated it as following:

$$\frac{L_D^2}{\tau}\frac{\partial^2 n(x)}{\partial x^2} - \frac{n(x)}{\tau} + \frac{I_o \alpha}{\cos(\theta_\lambda)} \exp\left[-\frac{\alpha x}{\cos(\theta_\lambda)}\right] = 0$$

  The term in the left defines the diffusive transport with τ as the exciton lifetime and n(x) as the exciton distribution over wavelengths, diffusion length is related to the exciton lifetime through the famous diffusivity equation:

$$D = \frac{L_D^2}{\tau}$$

  Where D is the diffusion constant. The next term of the newly modeled equation model the decay or relaxation of excitation. The exciton generation rate is represented in the third term, which is a marriage between the absorption coefficient (α) equation and the incident light correction angle (θ_λ) (figure 2.2.4). The intensity of light passing through a material is characterized by the following equation:

$$I(x) = I_o \exp\left[-\alpha x\right]$$

Where I_o is the incident light intensity, α is the absorption coefficient.

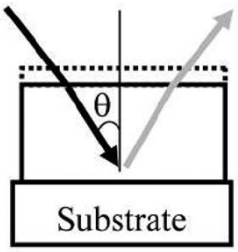

Figure 2.2.4. Dependence of exciton diffusion length equation on the angle of incident light (θ_λ) [36].

- Charge separation and transport efficiency (η_{CST})

  Exciton dissociation into free charge carriers, and the travel of these carriers is the following process. The scientific community did not settle on a specific mechanism in transport yet, and it is a topic of debate [37]. It is not clear if the charge transfer happens via an intermediate state, or a more direct relation that only require the electron affinities offset of the acceptor and donor to be larger than the internal columbic binding energy of the excitons. However, The separation process and the transfer from a donor to an acceptor LUMO's is considered to be fast and efficient process in OPVs [6].

- Charge collection efficiency (η_{CC})

  Designing the electrodes and selectively chose their materials is a matter of significance in order to achieve good collection of electrons. The relativity between the work function of the electrode material and the active layer polymer will dictate the charge collection efficiency parameter. Failing to optimize the electrode/active layer interface will cause an accumulation of unserviceable charges [38]. Aside from aligning the work functions and band edges, other techniques such as facilitating a buffer layer that block charges from going to the wrong electrode [39]. Figure 2.2.5 shows a band diagram of an OPV

cell with suitable work function alignment, and another device with buffer layers facilitated in it.

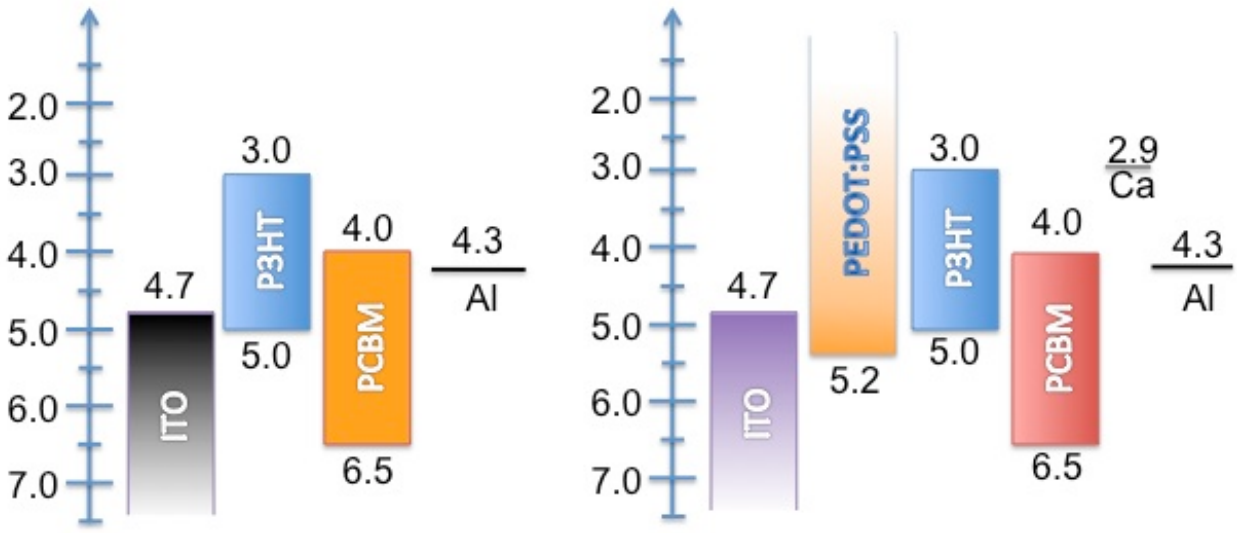

Figure 2.2.5. Band diagram of primitive OPV that may face a problem with wrong direction transport (left), and buffer-layer facilitated OPV (right), PEDOT:PSS block electrons from reaching ITO while Calcium block holes from reaching the Aluminum electrode.

Electrically, (J_{sc}) for OPVs has the same equation of regular photovoltaic. However, (V_{oc}) is slightly different from regular photovoltaic. An empirical equation was proposed after a study found a semi-linear relation between the measured V_{oc} of deferent BHJ compositions with the oxidation potential and the donor's HOMO position [40]. The equation is as following:

$$V_{oc} = \frac{1}{q}(|E^{Donor}HOMO| - |E^{Acceptor}LUMO|) - 0.3\,V$$

The value of 0.3 V is fitting factor; figure 2.2.6 shows a graph of V_{oc} in relation with the oxidation potential and the HOMO energy of the donor ($E^{Donor}HOMO$).

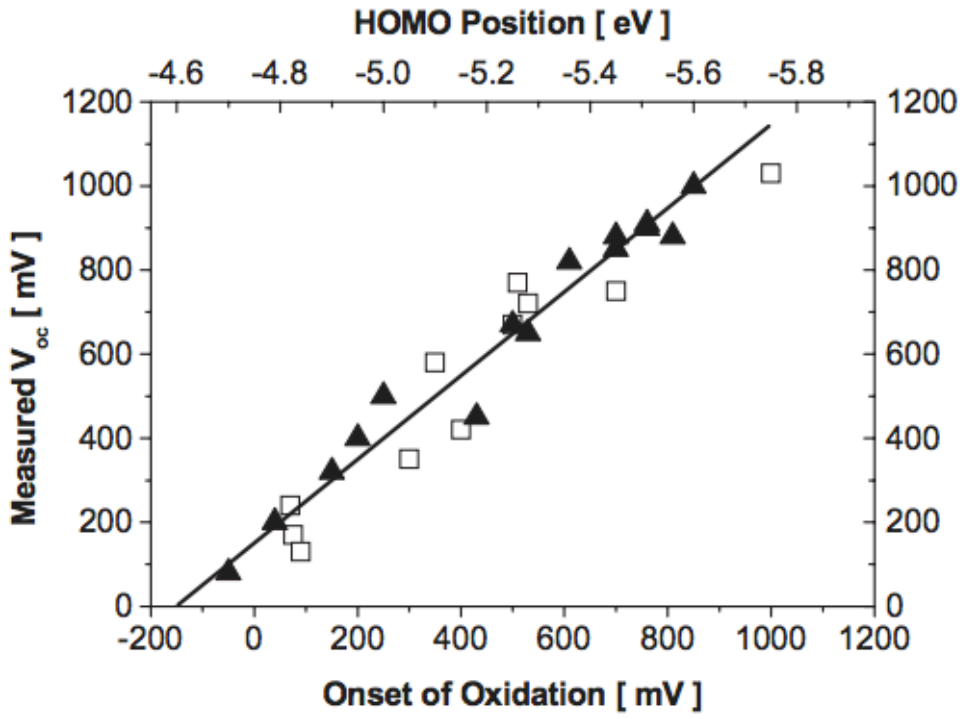

Figure 2.2.6. V_{oc} of deferent BHJ OPVs plotted against the oxidation potential/HOMO position of the donor material used in each OPV device [40].

2.3 Localized Surface Plasmon Resonance (LSPR)

In Nano scale Technologies, most materials that are contrived in such low dimensions experience modified and slightly different electrical and optical properties [41]. A major illustration is the phenomenon of localized surface Plasmon resonance (LSPR). LSPR is an optical phenomenon that takes place upon the interaction of metal Nanoparticles with light that has a wavelength larger than the Nanoparticles dimension. The oscillation of nanoparticles surface electrons (or conduction band charges) stimulated by light trapped in these nanoparticles, and thus a formation of localized electric field around the nanoparticle is the scientific argument behind LSPR (Figure 2.3.1) [42]. Hence, materials that have a high number of electrons on the conduction band such

as noble metals, or degenerately doped semiconductors will have a stronger appearance of LSPR (figure 2.3.2) [43].

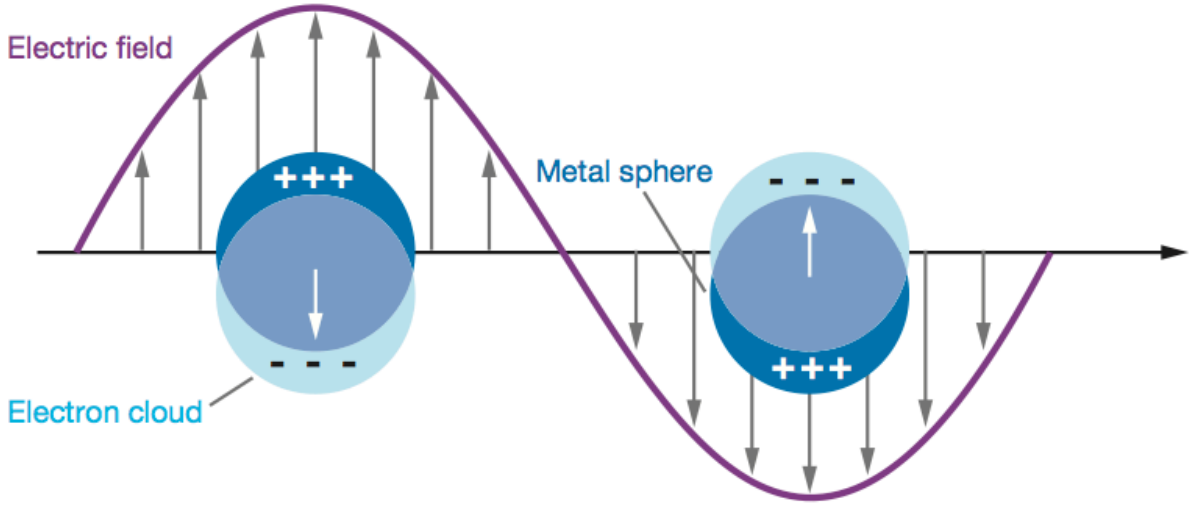

Figure 2.3.1. Oscillation of surface charges form an electric field that explains the LSPR [42].

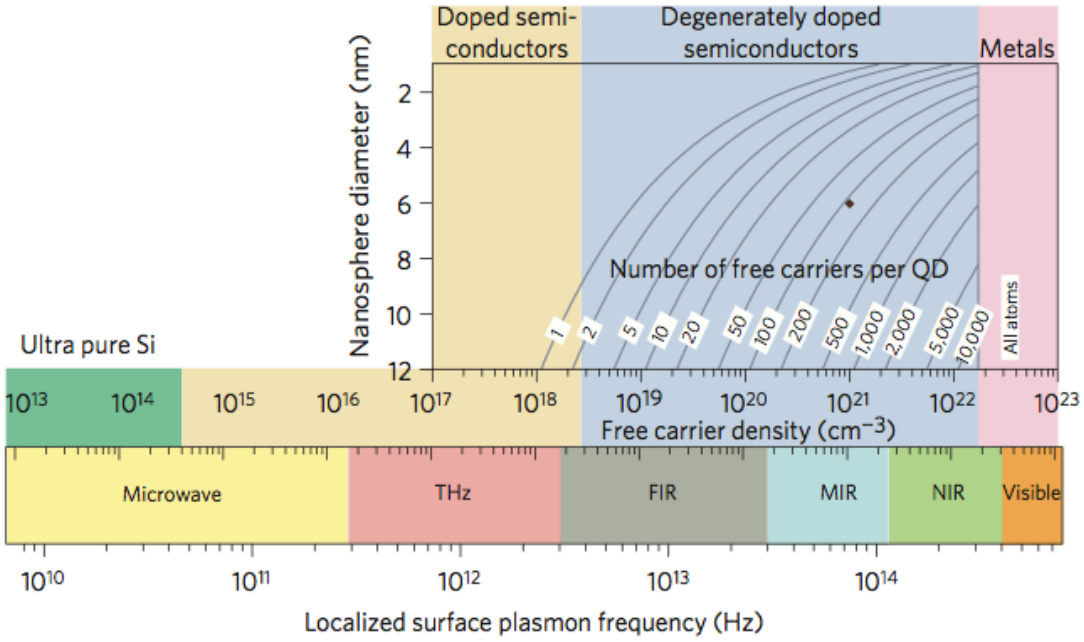

Figure 2.3.2. LSPR Frequency dependence on free carriers density [43]

LSPR is a highly tunable phenomenon, other than the material selection, the size, geometrical shape, spatial distance between particles, and dielectric environment are parameters that critically affect LSPR frequency [44]. Figure 2.3.3 represents the spatial deference dependency, while figure 2.3.4 present a total of 6 graphs that illustrate the shape and size dependency.

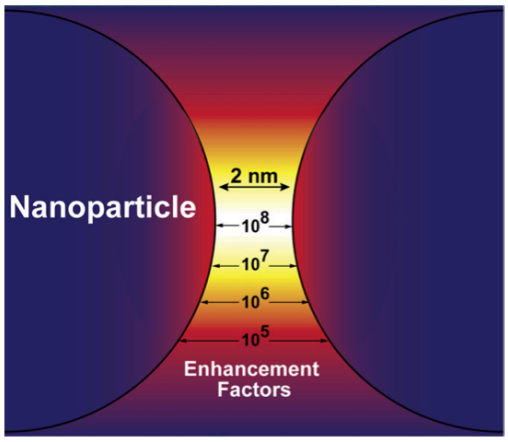

Figure 2.3.3. Spatial distance between particles affect the EM field in multiple order of magnitudes [44].

The LSPR peak frequency ω_{max} can be mathematically modeled and linked with the medium dielectric constants. Drude model can be adopted to find the Plasmon frequency as following:

$$\varepsilon_1 = 1 - \frac{\omega_p^2}{\omega^2 + \gamma^2}$$

Where $\omega_p \; and \; \omega$ are the plasma oscillation frequency and the light frequency respectively, ε_1 is the dielectric constant of the medium, and γ is a damping parameter of the bulk metal. For visible wavelengths, we can assume $\gamma \ll \omega_p$, and set $\varepsilon_1 = -2\varepsilon_m$ for the resonance condition, we can reach the following equation:

$$\omega_{max} = \sqrt{\frac{\omega_p^2}{1 + 2\varepsilon_m}}$$

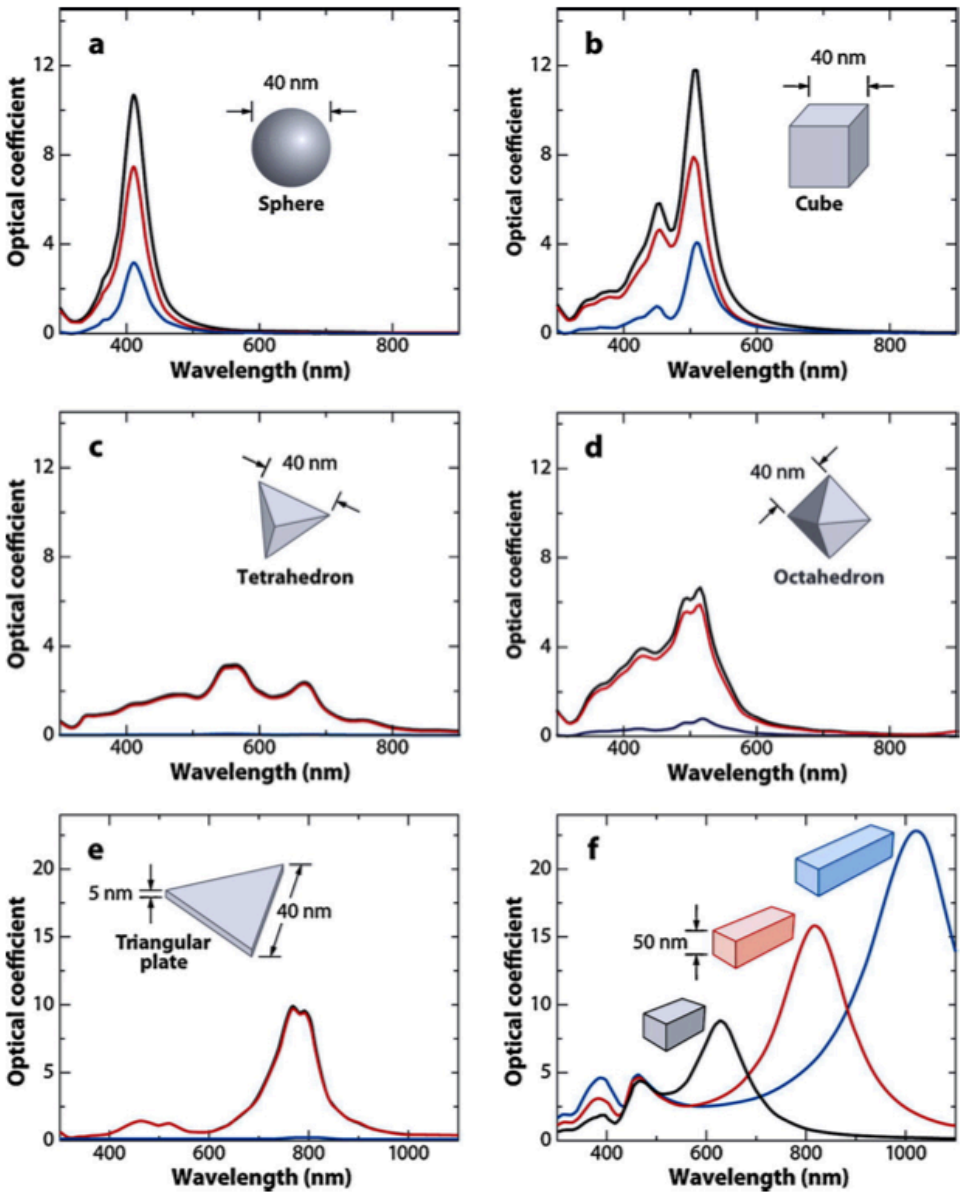

Figure 2.3.4. Absorption (red), scattering (blue), and extinction (black) spectra of silver Nanoparticles of multiple shapes. A) Sphere shows a single peak resonance, b-c-d-e) Cube, tetrahedron, octahedron, and triangular plate spectra, f) Extinction spectra of triangular bars with different aspect ratio. Extinction spectrum is the absorption spectrum added to the elastic light scattering spectrum [44].

A full analytical solution of Maxwell's equations for absorption and scattering of light by nanoparticles have been proposed by Gustav Mie [45, 46]. It is indeed very complicated to solve

the absorption and scattering properties for non-spherical shaped particles; that is to say that advanced electrodynamics numerical methods are being employed to obtain optical properties for such shape complicated particles.

3. Nano Pyramids Enhanced Organic Photovoltaic

Nano particles incorporated OPV researches have mostly focused on the layer of incorporation, and the particle sizes. The study of the nanoparticle geometrical aspect effect on OPV is a recent trend [47]. It is preferred to induce an OPV that has a better FF and PEC using shape manipulated metallic Nano particles. The shape we used is a pyramid structure, and we shall call it metallic Nano particles structure (NPY).

In this chapter, we will present the method used to fabricate an OPV cell, and grow metallic NPY on them. We will also demonstrate an increase in the FF of the OPV over non-Plasmonic OPV, and an enhancement of PCE over regular shaped nanoparticles OPV. We will also introduce three electron-conducting layers and study their impact on the cell parameters. Repetition and reliability analysis of fabricated cell will be discussed, proposed encapsulation method and measurement will be presented.

3.1 Device Fabrication

The regular OPV device made in DRL lab, Lies on an indium tin oxide (ITO) coated glass substrate. ITO, a transparent and conductive material, will serve as a hole-collecting end of the OPV. Although, Inverted devices (making the anode collect electrons instead of holes) have been suggested to enhance PCE [48-50], but we would rather apply our NPY structure on regular OPVs since these studies applied the inverted structure on tandem cells, in addition to the steady repetitive and reliability values of the regular OPV cell that we fabricate. The journey of OPV cell fabrication starts with a cleaning routine of the ITO-coated glass substrate that include manual scrubbing and lathering of special detergent on the substrate surface, followed by four 20 minutes interval of sonication in water solution of Sodium Hydroxide (NaOH), DI water,

($(CH_3)_2CO$ (acetone), and Isopropyl alcohol (IPA), respectively. The second step is to prepare the electron blocking layer, or the hole conducting layer (PEDOT:PSS) and spin coated in a spinner device, PEDOT:PSS (Baytron PVP Al 4083) is a black polymer that can be manipulated and doped [51] to acquire a certain work function values, and to have better conductivity [52] or transparency values [53]. The most important requirement of PEDOT:PSS is to have a suitable work function value that will build a more steep built-in potential to drive the holes into the anode. But nonetheless, studies on using (PEDOT:PSS) directly as an anode have shown some potential [54]. In contrast to employing (PEDOT:PSS) as an electron blocking layer, place it directly as an anode will require a good transparency vs. conductivity characteristic (e.g. $> 85\%$ transparency, and $< 30\ \Omega/\text{sq}$ resistivity).

For our work, the focus will be on having an influential work function instead of making direct anode (PEDOT:PSS). We have optimized the HTL to be having 70 nm-90 nm layer through sonication parameters of (2800 rpm for 1 min) followed by a backing of the coated substrate for 45 minutes under 130 C degrees, studies have shown better HTL performance after heat treatment due to film morphology modification, particle size modification, and conductivity modification [55]. On the same manner, deposition of BHJ absorption material (P3HT:PCBM) will be through spin coating using the spinner. However, a necessary transition from a regular vacuum hood environment into a high vacuum, and high quality glove box workstation has to take place.

The environment for the P3HT:PCBM photoactive layer and the metal electrode contact outside the glovebox is considered hostile, and the risk of oxidization of the active layer and the metal/active layer interface is lethal to the PCE value of the OPV devices [56]. The time needed to prepare the BHJ photoactive material is around 2 days, the first step of preparation is to mix

the powder of the P3HT and PCBM in clean vial in 1:1 ratio and dissolve the materials in Ortho-dichlorobenzene (ODCB) and have a final concentration of 40 mg/ml. 8-9 hours of heating (under 35 C) and stirring of the dissolved material will be the next step. Afterwards, spin coating of P3HT:PCBM BHJ blend on the previously coated PEDOT:PSS/ITO substrates. Since the absorption coefficient of P3HT:PCBM is high, the need for thick photo absorption layer is irrational. The optimization process of our Nano-layers device suggests a combination of two consecutive spins spans (600 RPM for 20 seconds, followed by 1100 RPM for 10 seconds). Annealing of the OPV device to form P3HT:PCBM islands to enhance conductivity and mobility is performed under 140 C degrees for about 6 minutes. Figure 3.1.1 shows the two working stations and some of the appliances used in the material and substrate preparation.

Figure 3.1.1. a) First stage to prepare OPV device, purification and super cleaning of ITO substrate using sonication

device on the left, followed by HTL deposition using spin coater device on the right. b) Purification system (high vacuum Nitrogen glove box) of the active layer depositing, photoactive layer is vulnerable to air and oxidization could plummet PCE.

The device is now ready for metal electrode coating. The metal evaporator chamber is integrated inside the high vacuum glove box to insure total device isolation from air or unwanted degradation causes. The metal used for the electrode in our device is Aluminum; it is worth mentioning that other research groups have tested thin silver layer, mono gold layer, and other types of electrode materials [57]. However, due to stability issue we will stick with Al as an electrode layer.

The evaporation chamber uses a tungsten connection to heat and evaporate the Aluminum precursor. The layer deposited is usually several tens of nanometer thick. We should mention that we usually deposit a thin calcium layer in like manner to the electrode deposition. The calcium layer will serve as an electron-conducting layer, since the calcium have a suitable work function to align with the device band structure. This step is just before the aluminum electrode deposition. The deposition will be through a stripped mask. Hence, each electrode strip will make up a device that can be tested and measured (Figure 3.1.2 a).

Our measuring setup consists of a connection circuit that will provide the connection to the OPV electrodes, a sun simulator that provide solar-spectrum like photon's wavelengths, and multimeters station to provide voltage and current readings. These data will be fed into a computer with a Labview interface to read, plot, and analyze the data. (Figure 3.1.2 b) shows a photo of several measurement devices.

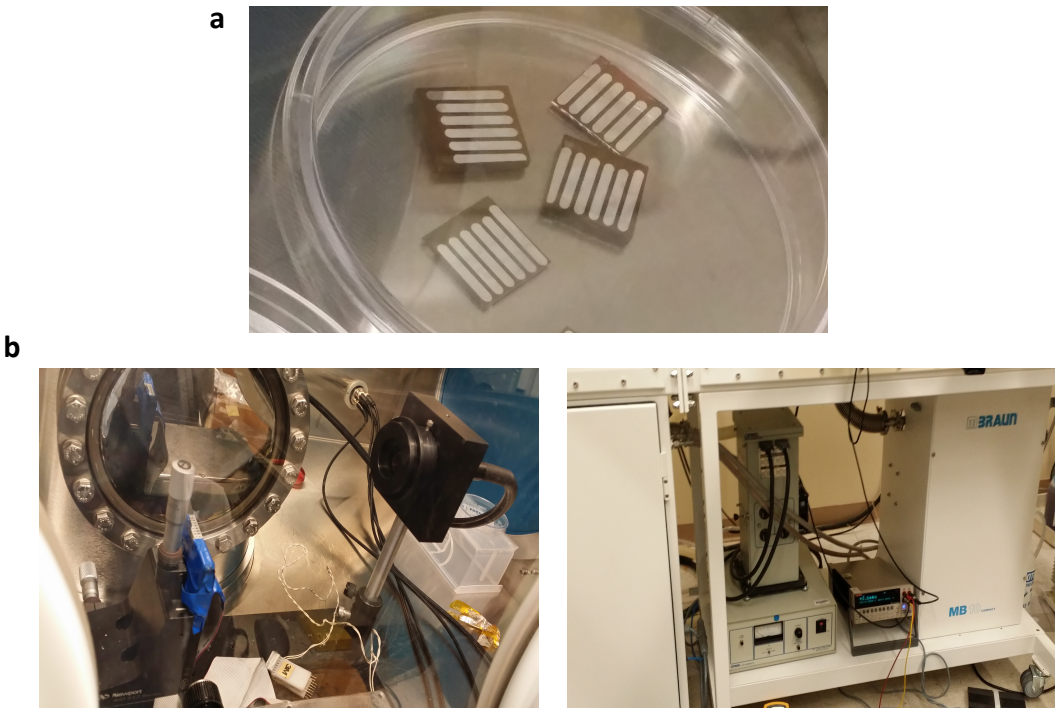

Figure 3.1.2. a) Electrode strips on a single OPV cell making 4 sub devices, device ready for testing and measuring.

b) Sun simulator (left), and multimeters setup (right) in our DRL lab.

Metallic Nano pyramids structure fabrication (NPY structure)

The Objective of fabricating the metallic nano particles is to employee the localized surface Plasmon resonance effect (LSPR) in our OPV device to increase the absorption, hence, increase the device efficiency. Figure 3.1.3 shows the process of growing NPYs in piecewise fashion.

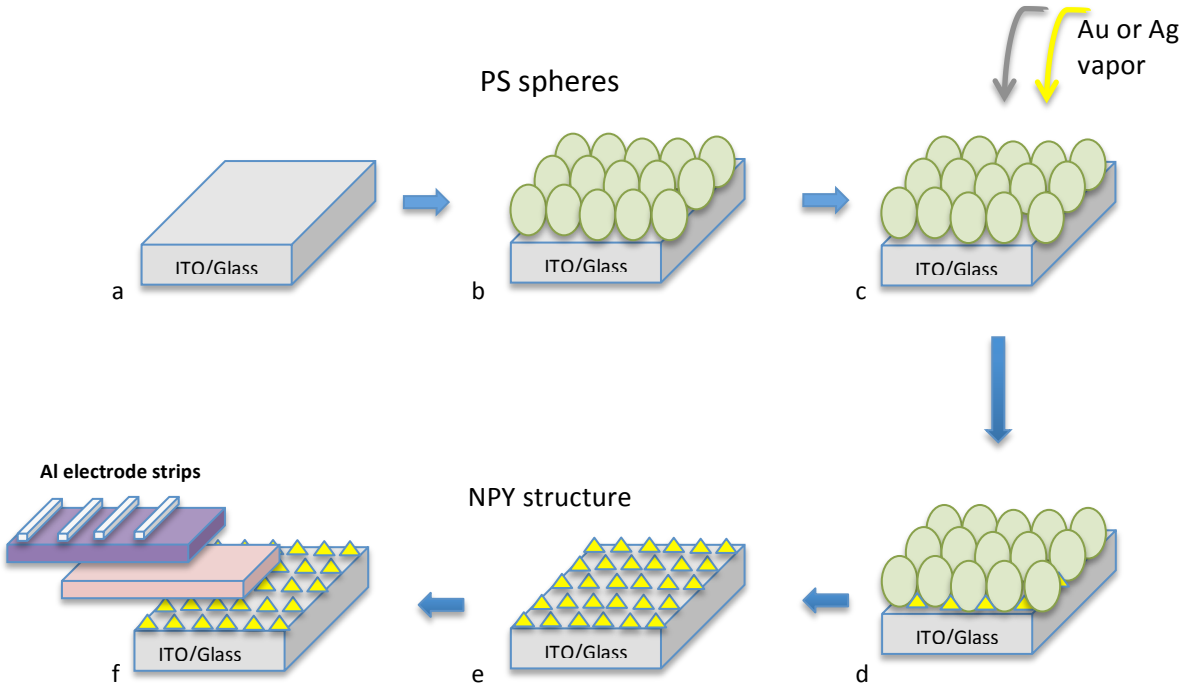

Figure 3.1.3. ITO/Glass substrate cleaned and ready for b) Polystyrene nanospheres deposition through nanoparticle lithography, followed by c) evaporating metal precursors and the resulting d) metal filling the voids. e) Removing the polystyrene spheres to end up with NPY structure and continue with f) depositing the other OPV layers.

The first process is to prepare a nanoparticles polymer solution called polystyrene spheres in order to start the nanoparticle lithography process. The preparation includes a dissolvent of polystyrene nanoparticle in ethanol in 1:1 ratio, followed by a diffusing of the solution on a DI water surface. The monolayer of polystyrene solution will start to form on the DI water. Afterwards, we will cautiously try to fish out the monolayer on the ITO/Glass substrate to avoid cracking it. A drying session will be followed to allow the polystyrene spheres to stabilize and

the solvent to vaporize. The next step will be taking the samples into the glove box station, specifically in the metal evaporation chamber. A session of evaporation of the NPY metal will take place. It is very important to keep the evaporation power in a low rating to avoid damaging the polystyrene sphere mesh. The metal vapor will start to fill the voids between the polystyrene spheres, which will normally make a pyramided structure. The height of the NPY structure is determined by the evaporator evaporation rate and time, it is only rational not to over fill the voids, which will cause a deviation in the shape of the layers. Figure 3.1.4 shows an SEM image of our polystyrene coated substrate.

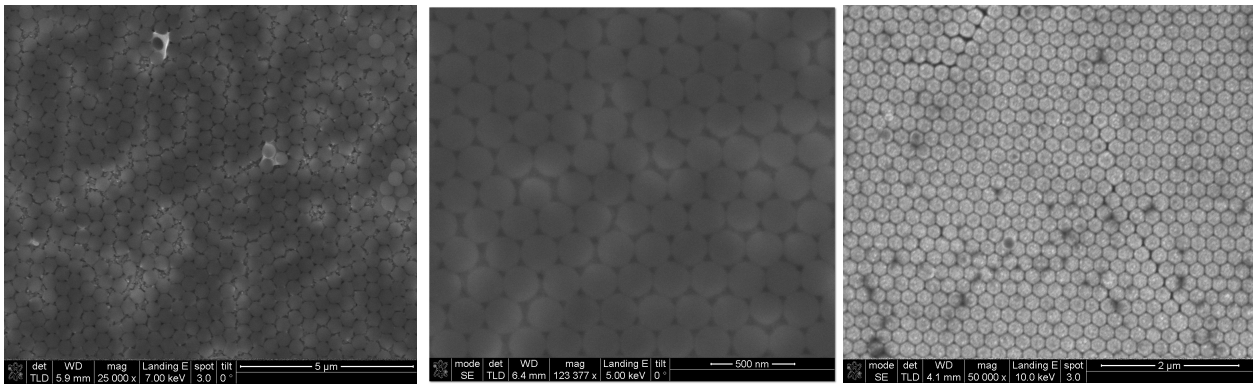

Figure 3.1.4. Polystyrene spheres coated on ITO/Glass substrate. The sizes of PS spheres are 450 nm (left) 270 nm (middle) and 100 nm (right).

We used different polystyrene spheres sizes, and found that a neater, and more compact shaped sphere occurs on the smaller sizes, and a percentage of deformation can take place when we go higher in size. The resulting NPY structure size can be correlated to the size of the polystyrene sphere sizes by the mean of geometry as following [58]:

$$L = \frac{1}{6}\pi D$$

Where L is the base side length, and D is the sphere diameter as figure 3.1.5 shows.

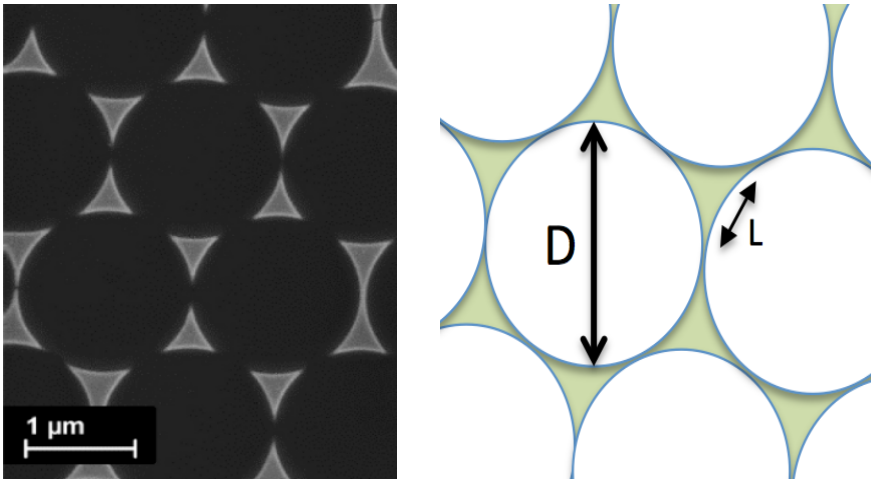

Figure 3.1.5. An SEM image and a schematic representation of NPY structure resulted from evaporating metal into closed-pack polystyrene sphere voids. D and L denote the PS sphere diameter and NPY base side length respectively.

However, it can be roughly rounded to 30% of the original polystyrene sphere size. It is very difficult to fabricate a well-compact and uniform structure. It rather contains some minor issues that can be neglected if it kept at minimum, issues such as NPY particles bridging, missed NPY particles, and a curvy or flat tips of NPY particles instead of the sharp shape. The issue of bridging can form if the polystyrene spheres are not homogeneous in size. It is hard to find a company that will provide polystyrene sphere sizes without any kind of deviation. The size given on the product data sheet is an average size, which means that a good product will have a good standard deviation value. As from our experience, Sigma Aldrich provide the best polystyrene spheres that were tried in DRL. Missed NPY particles can occur if the void between the spheres have been covered by another overlapping polystyrene sphere, second layer spheres is a very common problem, and the precaution is a very careful execution of the monolayer on the DI water surface. The flat NYP particles tip is almost an unavoidable problem, since it is almost impossible for such a structure to be form under the polystyrene lithography method, and the

only thing that can be done is to minimize the tip horizontal area to a minimum level (1 nm X 1 nm, or 5 nm X 5 nm). Figure 3.1.6 present some of the issue that faces NPY particles fabrication.

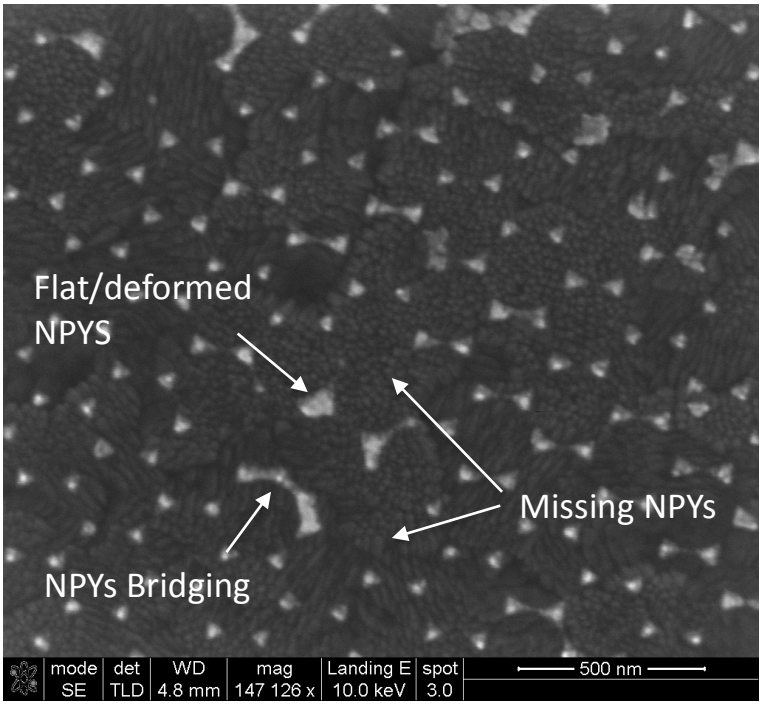

Figure 3.1.6. An SEM image of NPY structure with the most common problem faced with fabricating NPY structure (NPYs bridging, missing NPYs, and flat tip NPYs).

The importance of keeping a sharp tip of NPYs is to focus the LSPR around the NPY particles tip much higher than the regular all-around spherical particles LSPR. Hence, increasing the electric field around the tip and ultimately increase the absorption and power conversion efficiency. During the work, we found that it is extremely difficult and time consuming to form a monolayer of large polystyrene spheres ($> 1\ um$), and deploy it on the surface. Ironically, and in concept, the device should work better under smaller sizes of NPY particles (smaller polystyrene spheres) because in order to initiate the LSPR, you need nanoparticles that are smaller in geometry than the wavelength of light. The selection process of the NPY material had the following criteria; 1) the material should have a strong LSPR frequency, 2) the material peak

LSPR frequency should overlap with the wavelengths of the visible spectrum since the absorption window of the organic photo absorption layer (P3HT:PCBM, figure 3.1.7) is on the visible solar spectrum [59], and finally 3) the material can be fabricated in a nanostructure scale, and is adaptable to the Nano sphere lithography process to form Nano Pyramid (NPY) particles.

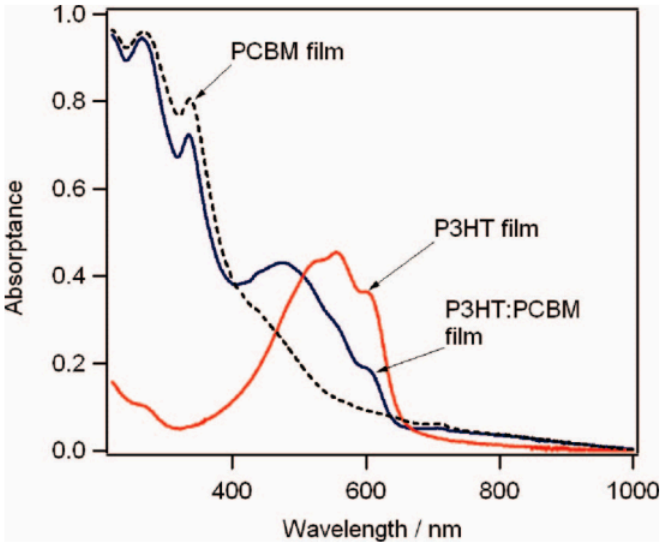

Figure 3.1.7. P3HT:PCBM Absorptance spectra, selected material for NPY should have an LSPR peak around the 500-600 nm wavelength region [59].

As an initial selection pool, noble metal such as Gold, Silver and Aluminum experience rich LSPR. As mentioned in the previous chapter, the LSPR is not only material dependent but rather multifactorial dependent. For the material selection we fixed every other factor that might affect LSPR, such as the intra-space between particles, the medium refractive index, the size, and shape. The selection came down to tow materials, Au and Ag. Silver has bigger amplitude of peak of LSPR, but yet it is very narrow and it has a wavelength of around 420 nm, which is at the edge of the absorption window of the active layer (P3HT:PCBM) [60]. On the other hand, Gold has a wide peak LSPR frequency, and covers a wide range of wavelengths (550-600 nm) that overlap with the active layer (P3HT:PCBM) absorption window[61]. However, the strength

of the gold LSPR is not as strong as the Silver peak LSPR. Fabrication wise, the silver NPY were very continent to fabricate and they formed a well-patterned NPY structure. On the contrary, Au NPY consisted of a lot of fabrication issues such as bridging and flat tips. Figures 3.1.8 and 3.1.9 show a contrast between Au and Ag LSPR frequency and an SEM image of Au/Ag NPY structures respectively.

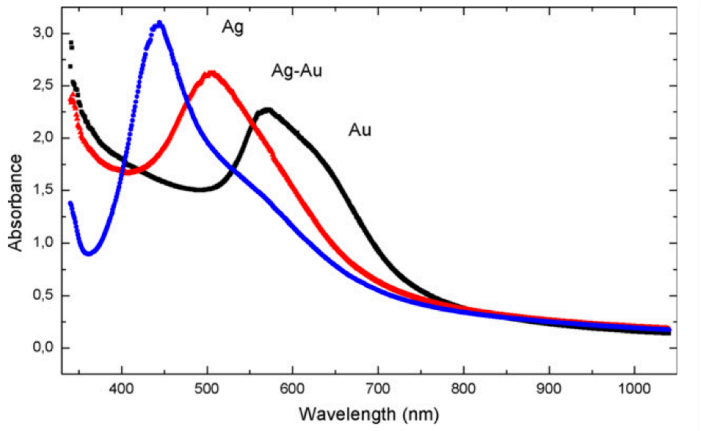

Figure 3.1.8. P3HT:PCBM absorptance spectra, selected material for NPY should have an LSPR peak around the 500-600 nm wavelength region, the size of the tested particles is less than 150 nm, all other factors have been fixed [61].

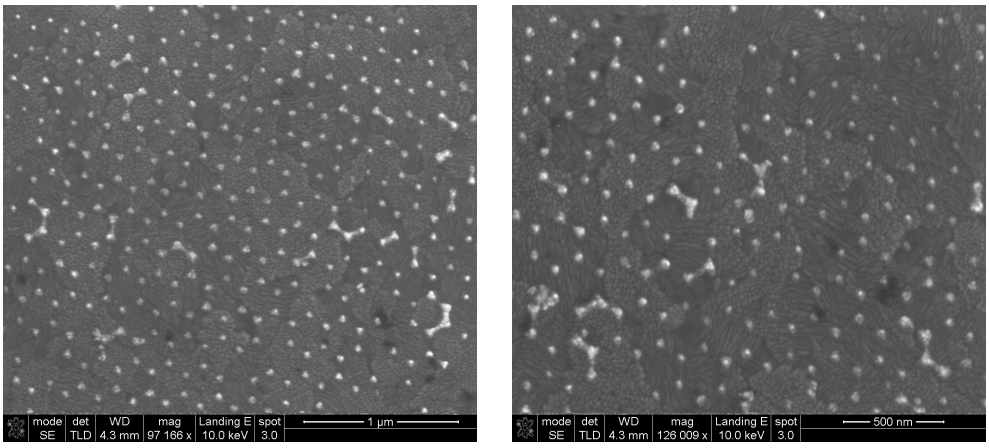

Figure 3.1.9. Silver NPY structure has a better-shaped and more compact structure (lift). Gold NPY structure contains defects such as missing NPYs and bridging between NPY units (right).

3.2 Experimental Measurements

As the previous section shows, the process of fabricating an organic photovoltaic is not very complicated, however, it is long and not so straightforward either. Each step had to be optimize, and that step could be modified if we found that the next step would not interact well with the previous one. The optimization process took place in a step-by-step approach, and then modified to be couple of step by couple of step approach, and at the final stages we tried to collectively optimize the device through optimizing several parameters simultaneously. The first step was to optimize the NPY structure size, separation, and height. The following optimization stage was to optimize the thickness of the HCL (PEDOT:PSS), the thickness of the (PEDOT:PSS) can be optimized by optimizing to factors, which are the speed of rotation of the spin coater (rpm), and the spinning time. By the same token, the third stage is the optimization of active layer thickness and solvent ratio (P3HT:PCBM). Afterward is the optimization of the HBL thickness and material selection, and finally optimizing the electrode thickness and material selection. It is important to sustain a steady repetitive power conversion efficiency of cell. In our experience, we have kept my devices in a suitable efficiency region of around (3.6%) and a standard deviation of about 0.09%. Figure 3.2.1 and 3.2.2 shows the voltage-current density curve of ten devices that were fabricated consequently in a specific time and the correspondent power conversion efficiency and fill factor of each device, the IV curve is totally overlapping for the 10 devices in the fourth quadrant, which in other words mean an overlapping of open circuit voltage and short circuit current, the open circuit voltage and short circuit current will determine the efficiency of the device in line with the maximum power point which was also overlapped.

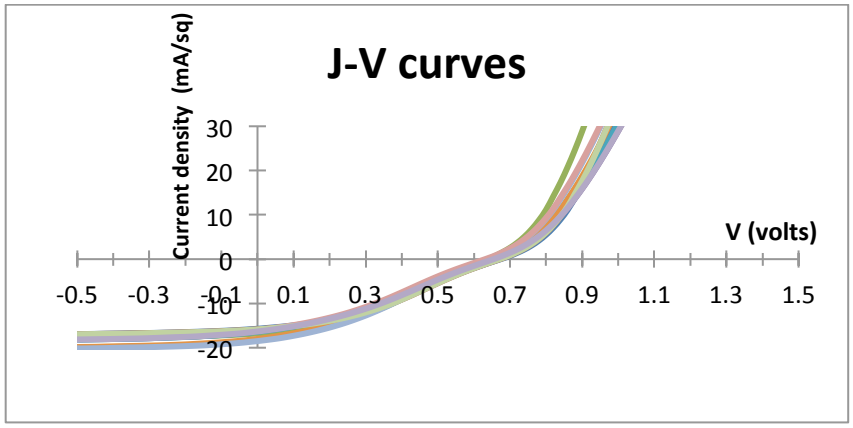

Figure 3.2.1. J-V curve of ten devices fabricated consequently. The statement that we can make is that in any given time, and if we decided to fabricate 10 devices, their measurements will be in that range.

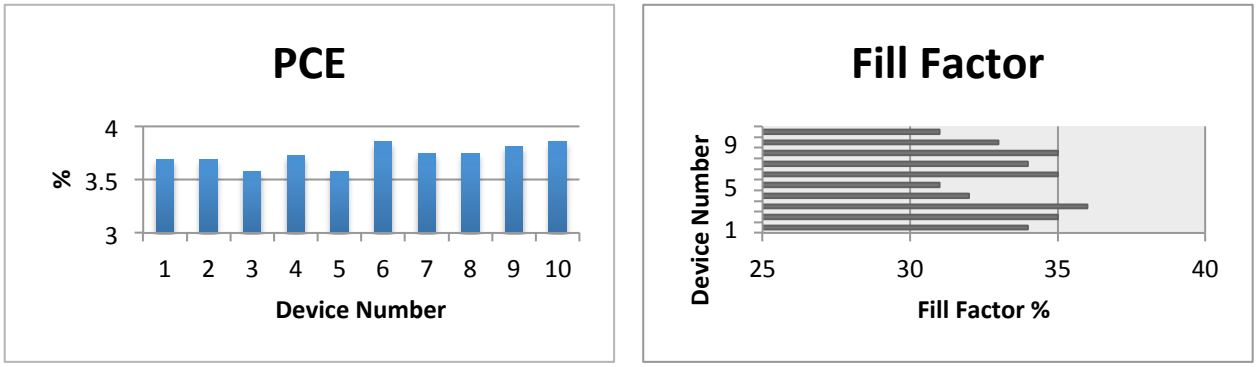

Figure 3.2.2. The range of Power conversion efficiency and fill factor of 10 any-time fabricated devices.

The power conversion efficiency has sustained 0.01% difference between the ten devices, which indicate reliable and optimized fabrication process. Fill factor witnessed a sense of reliability too, with all of the devices ranging between 32-37% FF. It is almost impossible to keep a zero variation parameters. However, with proper and narrow fabrication technique, the variation between devices can be minimized. Figure 3.2.3 presents the JV curve of 2 devices, one that contains Au NPY particles and the other contained Ag NPY particles.

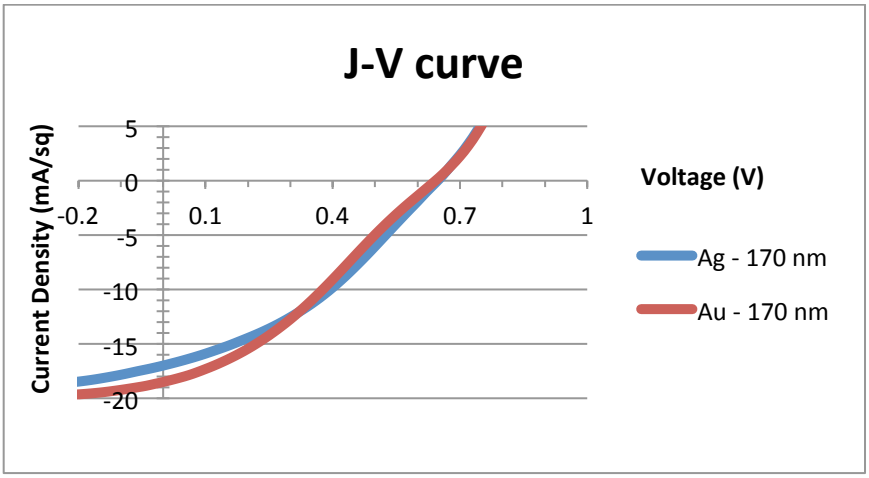

Figure 3.2.3. The JV curve of OPV incorporated with different materials of NPY materials.

As expected the Au will out perform the Ag NPY structure in the J_{sc}values since the Plasmonic resonance peak of the gold overlap with the absorption window of the active layer (P3HT:PCBM). At the same time, we have the V_{oc} untouched since it is mainly controlled by the HOMO-LUMO energy level difference and the amount of incident light. The efficiency is correlated to J_{sc} and it is expected to rise, however the fill factor did not vary greatly, since the maximum power point did not vary greatly between both NPY materials. Figure 3.2.4 shows the efficiency and fill factor values of both OPV devices while incorporated with different NPY materials.

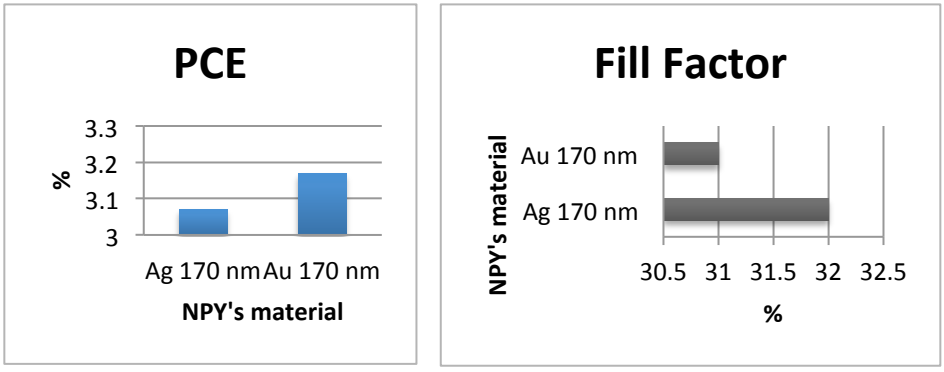

Figure 3.2.4. Efficiency and fill factor ratings of OPV device incorporated with different NPY materials.

Consecutive to the efficiency dependence on the material study, we will present our result of the NPY size dependence. The polystyrene Nano sphere sizes tried in the lab are 1.1 um, 0.95 um, 0.65 um, 0.46 um, 0.3 um, and 0.16 um, which will result into an NPY sizes of 300 nm, 250 nm, 170 nm, 120 nm, 80 nm, and 42 nm respectively. Figure 3.2.5 and 3.2.6 shows the JV curve and the efficiency and fill factor ratings dependence on incorporated NPY particle sizes.

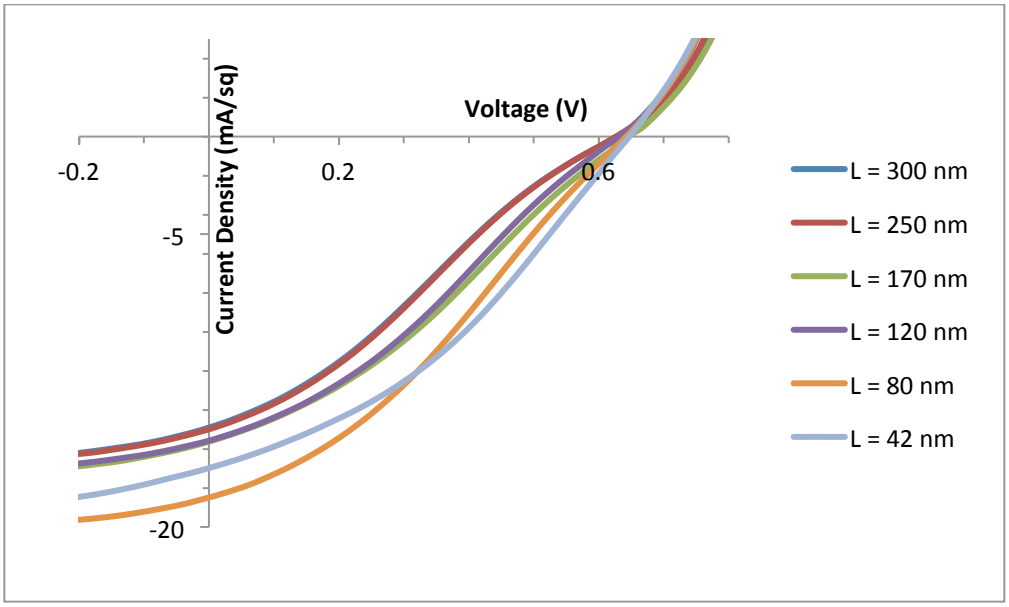

Figure 3.2.5. Dependence of short circuit current and maximum power point on the size of NPY particles.

In line with theory, as we shift toward smaller nanoparticle sizes the peak Plasmonic resonance frequency shift too. The shift is actually toward the absorption window, and hence, the absorption enhancement will initiate and the coupling will be even stronger. The previous graph shows that J_{sc} is getting larger as we grow smaller NPY structures. As mentioned earlier, the efficiency is directly dependent on the J_{sc}. Therefore a growth in efficiency is expected, and the following bar chart presents that.

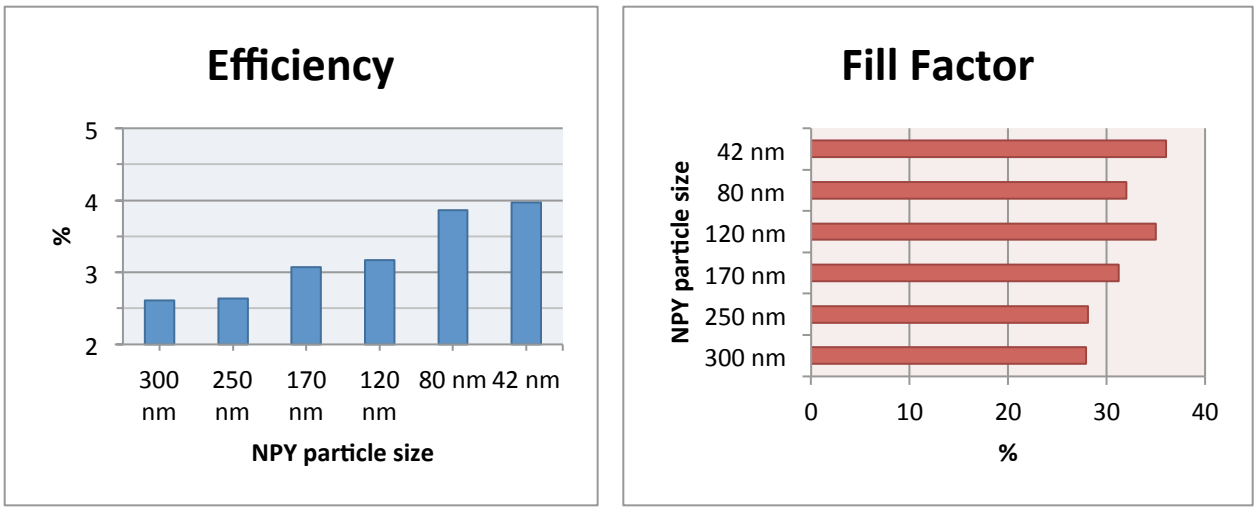

Figure 3.2.6. Dependence of efficiency and fill factor on the size of NPY particles.

The fill factor is directly dependent on the maximum power point, and because of the minimum variation in respect to the NPY structure size, we did not witness breakthrough enhancements. Nevertheless, a noticeable increase took place between the 300 nm NPY size and 42 nm NPY size. Even more, the smaller size of NPY structure will reflect less incidents light than their counter larger NPY sizes (Figure 3.2.7). Additionally, smaller sizes usually have less defects and deformation such as NPY particles bridging, NPY flat tip, or missing NPY particles, this issue was discussed in details in the fabrication process section.

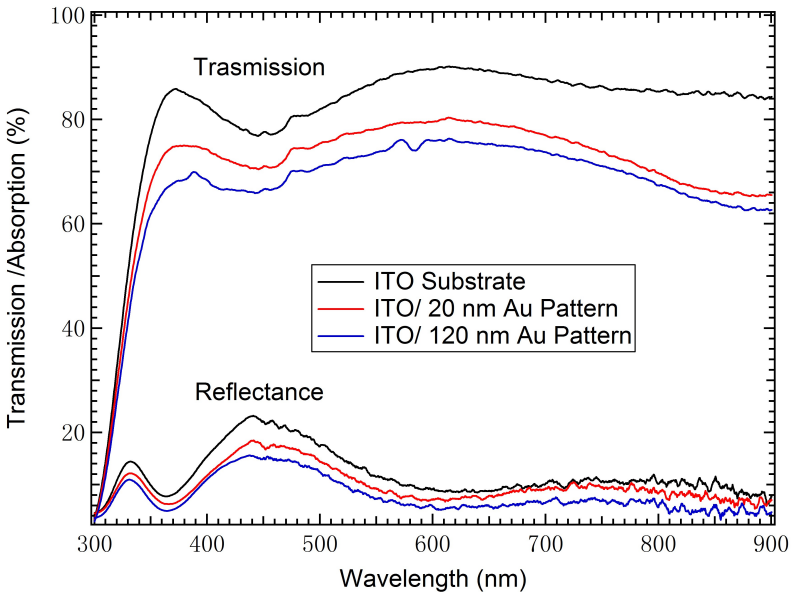

Figure 3.2.7. Reflectance and Transmittance graph of 2 NPY structures, smaller structure reflects less light and allow light to penetrate more efficiently. Note that smaller structure is the red curve (120 nm and 20 nm are the spatial distance between NPY units, and not the actual size of NPY units)

The shape of the Nano particle is also decisive, and can contribute either positively or negatively. Figure 3.2.8 shows the deviation between regular spherical shaped nanoparticles and our NPY structure in terms of JV characteristic.

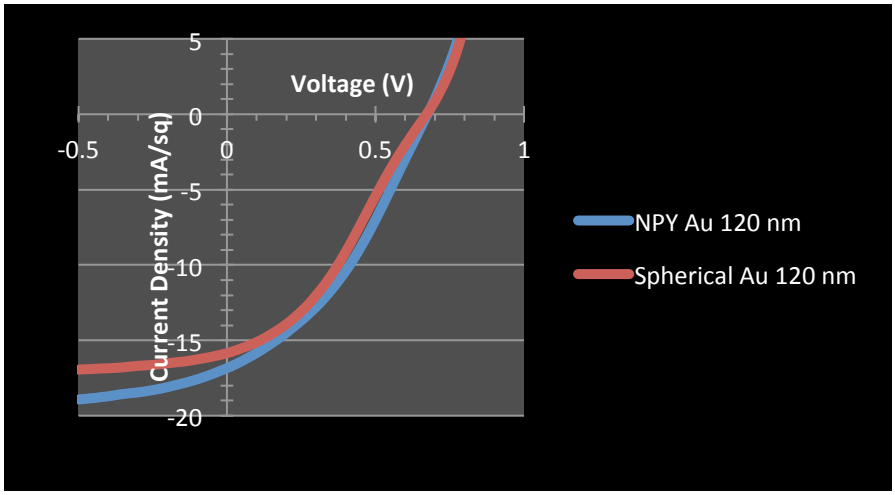

Figure 3.2.8. Shape dependence of nanoparticles on the JV characteristic curve.

The graph shows an increase in both J_{sc} and maximum power point ratings. And as a consequence, both efficiency and fill factor readings were enhanced. The enhancement can be regarded to the aided plasmonic resonance by the specially shaped NPY particles. The monumental difference between spherical, random shaped nanoparticle and their special geometrical NPY particles is the ability to aid the plasmonic enhancement field in the tip of the pyramids instead of the all-round enhancement. Finite-Difference Time-Domain (FDTD) method was applied to simulate the electric field enhancement around the Nano particles. In figure 3.2.9, you can notice the difference between the electric field enhancement between the spherical shape and the pyramidal shape in a pattern structure.

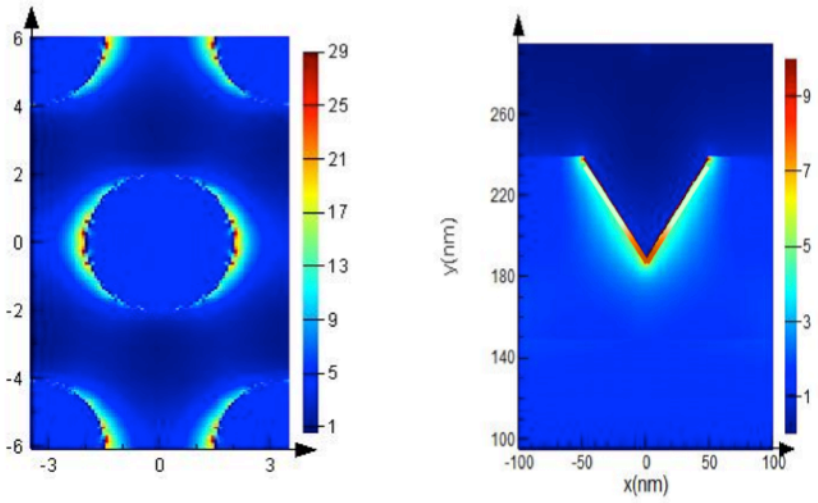

Figure 3.2.9. Electric field distribution in spherical and pyramidal metallic nanoparticle structure, enhancement is more focused on the tips of the NPY.

3.3 Electron Conducting Layer

In this section we present three different organic interlayer materials:1,2-Dipalmitoyl-sn-glycero-3-phosphocholine (DPPC), polyethyleneimine ethylene diamine branched M_w~800 (PEI), and

Poly(9,9-bis(3'-(N,N-dimethyl)-propyl-2,7-fluorene)-alt-2,7-(9,9-dioctylfluorene)) (PFN), that we studied their effect during the previous period. The importance of electron conducting layer research is to find alternatives to aid the charge carriers to be collected efficiently, and hence, increase both the charge transport efficiency (η_{CT}) and charge collection efficiency (η_{CT}). DPPC was selected since the head group of the polymer has an intrinsic dipole moment supporting the electric field of the cell, and the aliphatic tail will bind it to the surface of the active layer through Van der Waals force. PEI has been shown to lower the work function of an ITO electrode In previous work, making it a suitable cathode for inverted OPVs [62]. In our work, we use PEI as an electron-conducting layer between the active layer and the aluminum cathode. Cao *et al* [63] have already confirmed the usefulness of PFN as an electron-conducting layer with other polymer systems. The mechanism of enhancement for both PEI and PFN could arise from a combination of the formation of a dipole as well as a decrease in the work function of the metal. The used OPV in this study is made with (P3HT:PCBM) system. Figure 3.3.1 and 3.3.2 shows a schematic of the OPV cell with included interlayer, and the compounds structure respectively.

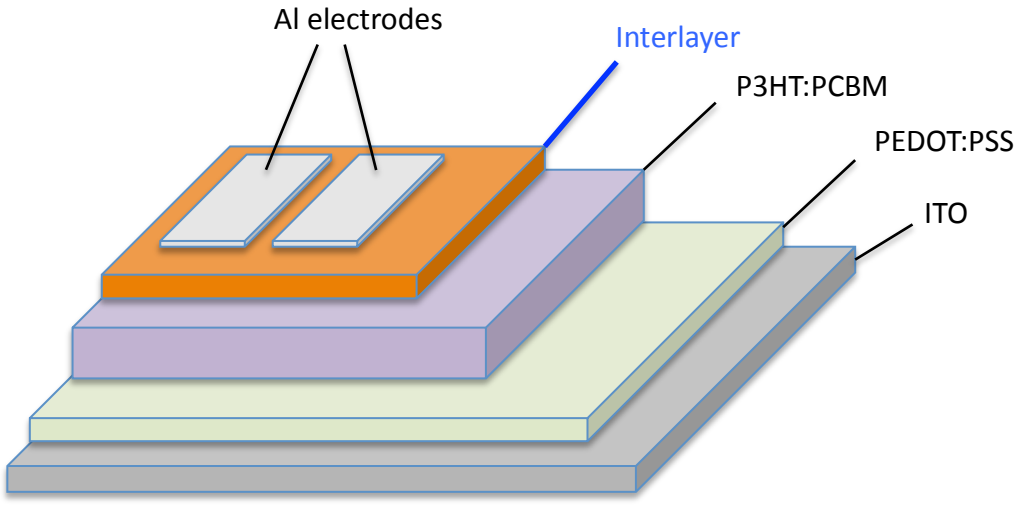

Figure 3.3.1. Cartoon showing the interfaces of the tested layer of the OPV device.

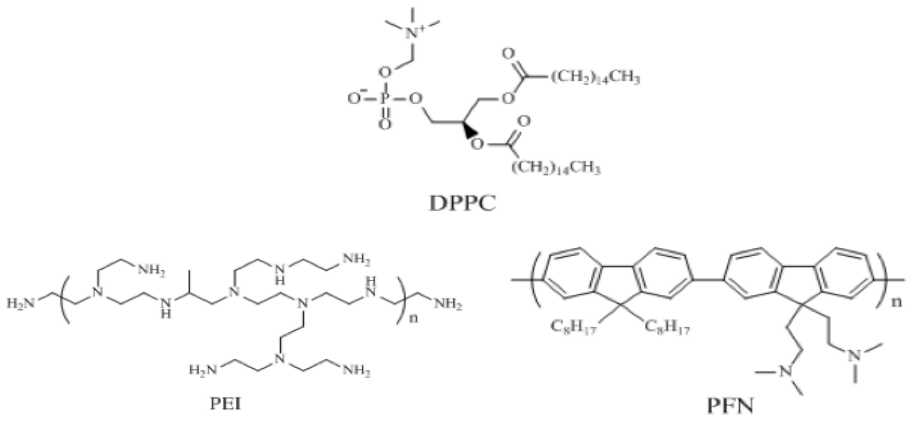

Figure 3.3.2. Cartoon showing the interface of the tested layer of the OPV device.

The materials were bought from Sigma Aldrich and material 1, and used as is with no further modification. The parameter for the interlayer is shown on the table on figure 3.3.2, the outcomes demonstrate that all of the examined layer materials have appreciably improved the performance of the cell.

	DPPC	PFN	PEI	Al only
Solvent	Ethanol	Methanol	IPA	
Concentration (mg/ml)	0.5	0.27	0.25	
Spinner speed (rpm)	4000	500	4000	
Open circuit voltage (V_{oc})	0.54	0.55	0.55	0.371
Short circuit current density (J_{sc})	10.4	10.4	10.3	9.95
Fill Factor	63.2	61.7	58.8	45.1
Efficiency	3.52	3.5	3.33	1.67

Figure 3.3.3. Table showing the parameters (spinning speed, V_{oc}, J_{sc}, FF, and PCE) affected by adding the interlayers of (DPPC, PFN, and PEI). DPPC has outperformed PFN and PEI, however all of them have shown considerable increase

With DPPC showing the highest and PEI having the lowest enhancement. It is important to mention that the PEI and DPPC interlayers are thin and can be categorized as (monolayer), as the layers become thicker the cell drops drastically in performance. However, PFN performance did

not appear to be affected by the thickness, and it sustained similar parameter with increasing thickness. The study was done on (P3HT:PCBM) system only, other narrow band gap organic semiconductors are in line for testing. The significant boost in efficiency cannot be neglected and shall be hybridized with other approaches to boost the power conversion efficiency.

3.4 Encapsulation

Genetically, organic photovoltaic are vulnerable to degradation from air, water, and moister molecules, which will make the lifetime of the OPV outside the glove box station very limited. Numbers of studies have looked into this issue [64, 65], and it is currently one of the main paths toward achieving high-efficiency, long lifetime, fixable organic solar cell. We have tried an encapsulation material (Cytop) that proved efficiency sustainability for over than 1000 hours [66]. Figure 3.4.1 and 3.4.2 shows the effect of degradation on OPV and in contrast with encapsulated OPV on the following parameters: V_{oc}, J_{sc}, FF, and PCE versus time.

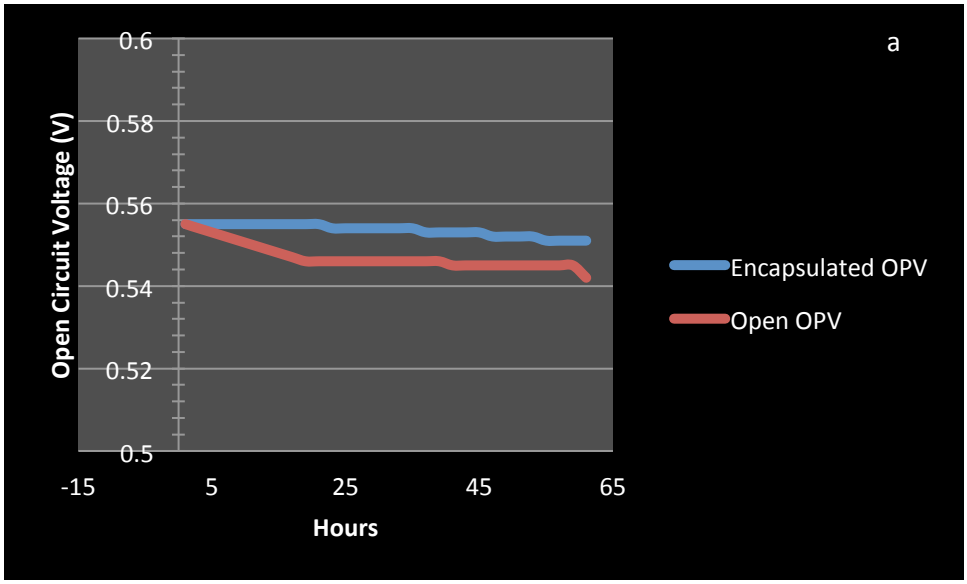

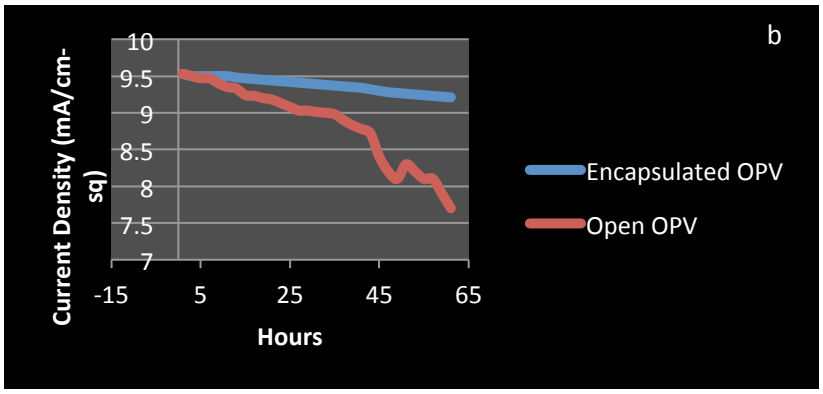

Figure 3.4.1. a) V_{oc} relatively kept the value over 0.5 V for both cases. b) J_{sc} plummeted before the 24-hour mark for the open case sustained old levels in encapsulation.

Although the open circuit voltage kept its value relatively sustained over the 60 hours period, the drama took place in the short circuit current value, before the 24-hour mark the value has plummeted in about 10% and by the 60-hour mark the J_{sc}has reached 7.5 mA/cm^2, which is about 30% reduction from the original value.

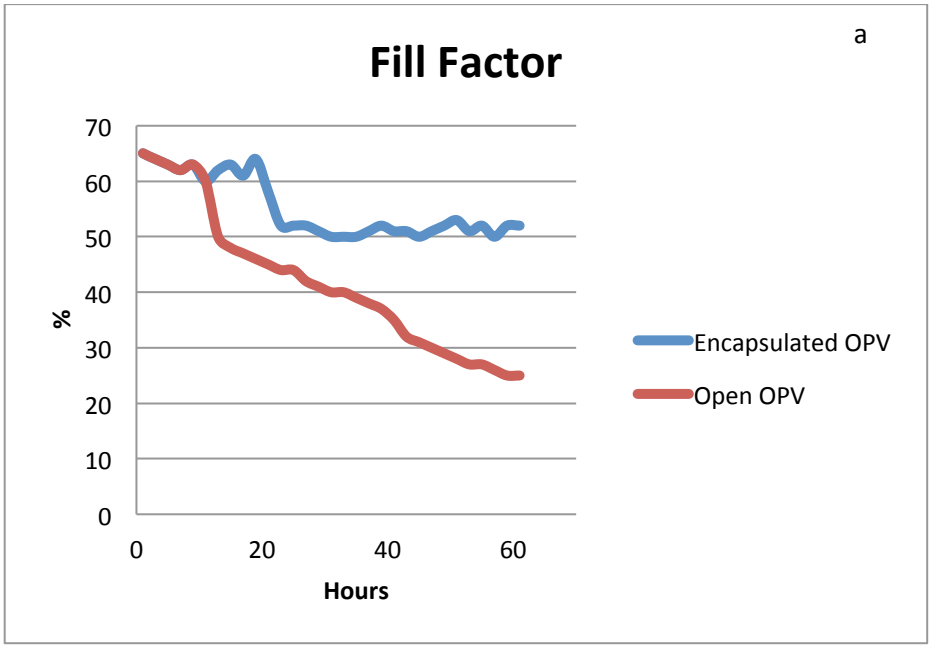

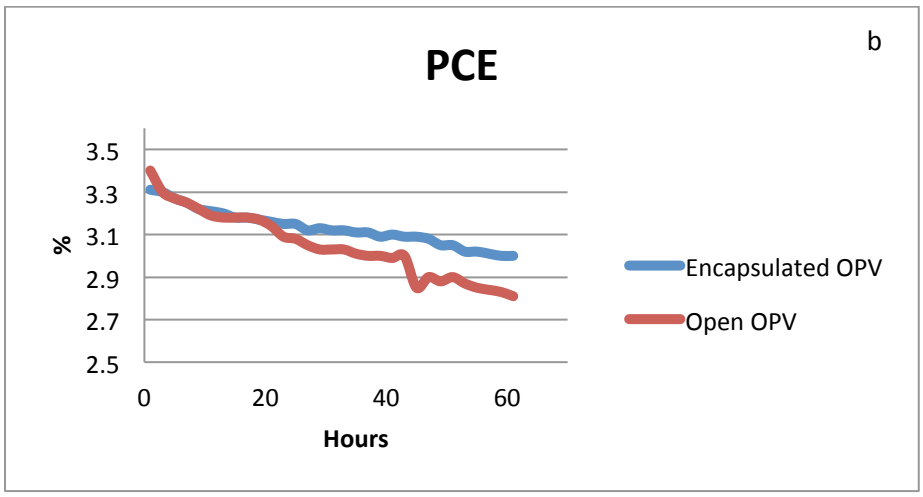

Figure 3.4.2. FF and PCE experienced similar degradation effect to the J_{sc}.

The drastic reduction of J_{sc} has affected the values of power conversion efficiency and fill factor in similar fashion. Nonetheless, the encapsulated cell with Cytop (figure 3.4.3) has kept the values of J_{sc}, FF, and PCE in less than 5% reduction. All in all, encapsulation techniques are a necessity since the only place for the OPV to live is inside the workstation. Encapsulating OPVs with Cytop have been done many times, we have verified the process and studied the effectiveness on our NPY OPV device and found the encapsulation to be effective.

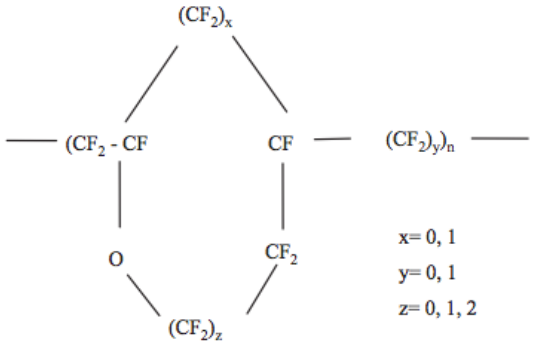

Figure 3.4.3. Compound chemical structure of the encapsulating material (Cytop) [68].

4. Nano Pyramid Pattern on the Electrode Side

Currently, we are trying to achieve depositing the NPY structure on the interface between the active layer (P3HT:PCBM) and the electrode (Al). In addition to the plasmonic effect they provide, the advantages of incorporating the NPY structure in the electrons path interface are 1) enhanced management of light, since the light will be reflected from the back NPY structure into the active layer, and 2) provide a passivation factor to the Aluminum/Active layer interface to reduce degradation through oxidization, since the NPY materials is usually Au, or Ag. Primary sets of result have shown short-circuited device results. Our assessment is that the NPY particles are penetrating and fracturing the photoactive layer and starting a short circuit process (Figure 4.1.1). Protrusion through the active layer can be minimized theoretically by fabricating less sharp-tip NPY particles. Less sharp-tip NPY can be manufactured by increasing the intra space between polystyrene spheres, however, it is a difficult process since the remote spaced polystyrene sphere will not result into a Nano pyramid structure, they will rather form a mesh of Au or Ag layer with openings that represent the place of the Nano spheres. Unless NPY particles are in the Nano scale, and are dispersed with intra space between them, the Plasmonic effect will not initiate. The idea is currently under investigation and troubleshooting process by our team.

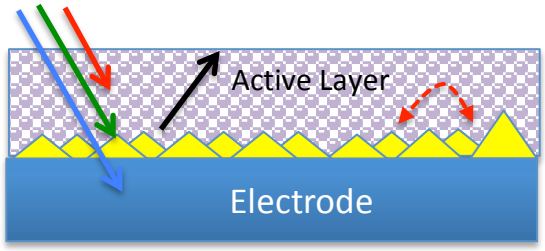

Figure 4.1.4. Introducing the NPY structure into the back electrode bring an advantage and a drawback. The advantage is that NPY structure reflects some of the incident light into the active layer again in addition to the

absorption enhancement they provide, the drawback is the formation of recombination traps and ultimately cause electron-hole annihilation.

5. Conclusion

Plasmonics are opening a path for the boosting of the solar cell's internal and external quantum efficiencies, especially in the organic photovoltaic field. The analysis of the Plasmonic effect dependence on the geometrical aspect of the Nano particles have been studied abstractly before, however, integrating unique shaped Nano particles along with their distinct Plasmonic behavior into organic photovoltaic is infrequent and very little in numbers. The empowering of organic photovoltaic through Plasmonic effect can make them convenient candidates for numerous energy-need applications, applications such as photons exploiter of the screens of portable devices since the transparency is a major advantage of the OPV, or to integrate it with other foldable and rollabale accessories since flexibility is another key advantage. Our NPY structure OPV can be further investigated by incorporating the pyramidal structure into a different layer or interface. Moreover, fabricating other geometrical designs such as half-spheres, three layers cylinders of metal/semiconductor/metal, or flat-tip pyramidal particles can open up new study paths. In our device, we have determined that NPY structure have increased the overall efficiency of the OPV when compared to devices with regular shaped Nano particles, we have also optimized the material selection, the base size, and the height of the NPY particles. Moreover, we have presented a new electron-conducting layer that will promote the internal quantum efficiency, and conducted the optimization process of the proper material thickness and solvent concentration. We are currently on the progress of growing the NPY structure on the back electrode/ active layer interface, we are trying to overcome the short circuit results by passivizing the NPY particles tip to prevent them from acting as a recombination centers. All in

all, eccentric shaped Nano particles could offer a great potential to enhance the organic photovoltaic efficiencies and hence, hold a great potential to be deployed in numerous technology application.

6. References

[1] G. Dennler, M. C. Scharber, and C. J. Brabec, "Polymer-Fullerene Bulk-Heterojunction Solar Cells," *Advanced Materials,* vol. 21, pp. 1323-1338, 2009 2009.

[2] G. Li, R. Zhu, and Y. Yang, "Polymer solar cells," *Nat Photon,* vol. 6, pp. 153-161, 2012/03// 2012.

[3] H. Shirakawa, E. J. Louis, A. G. MacDiarmid, C. K. Chiang, and A. J. Heeger, "Synthesis of electrically conducting organic polymers: halogen derivatives of polyacetylene, (CH)," *Journal of the Chemical Society, Chemical Communications,* pp. 578-580, 1977 1977.

[4] H. Shirakawa, A. G. MacDiarmid, and A. J. Heeger, "Twenty-five years of conducting polymers," *Chemical Communications,* pp. 1-4, 2003 2003.

[5] S. Glenis, G. Horowitz, G. Tourillon, and F. Garnier, "Electrochemically grown polythiophene and poly(3-methylthiophene) organic photovoltaic cells," *Thin Solid Films,* vol. 111, pp. 93-103, 1984/01/13/ 1984.

[6] N. S. Sariciftci, L. Smilowitz, A. J. Heeger, and F. Wudl, "Photoinduced Electron Transfer from a Conducting Polymer to Buckminsterfullerene," *Science,* vol. 258, pp. 1474-1476, 1992/11/27/ 1992.

[7] N. S. Sariciftci, D. Braun, C. Zhang, V. I. Srdanov, A. J. Heeger, G. Stucky*, et al.*, "Semiconducting polymer–buckminsterfullerene heterojunctions: Diodes, photodiodes, and photovoltaic cells," *Applied Physics Letters,* vol. 62, pp. 585-587, 1993/02/08/ 1993.

[8] G. Yu, J. Gao, J. C. Hummelen, F. Wudl, and A. J. Heeger, "Polymer Photovoltaic Cells: Enhanced Efficiencies via a Network of Internal Donor-Acceptor Heterojunctions," *Science,* vol. 270, pp. 1789-1791, 1995/12/15/ 1995.

[9] W. Ma, C. Yang, X. Gong, K. Lee, and A. J. Heeger, "Thermally Stable, Efficient Polymer Solar Cells with Nanoscale Control of the Interpenetrating Network Morphology," *Advanced Functional Materials,* vol. 15, pp. 1617-1622, 2005/10/01/ 2005.

[10] S. H. Park, A. Roy, S. Beaupré, S. Cho, N. Coates, J. S. Moon*, et al.*, "Bulk heterojunction solar cells with internal quantum efficiency approaching 100%," *Nature Photonics,* vol. 3, pp. 297-302, 2009/05// 2009.

[11] Y. Liang, Z. Xu, J. Xia, S.-T. Tsai, Y. Wu, G. Li*, et al.*, "For the Bright Future—Bulk Heterojunction Polymer Solar Cells with Power Conversion Efficiency of 7.4%," *Advanced Materials,* vol. 22, pp. E135-E138, 2010/05/25/ 2010.

[12] D. Arvizu, "Solar Photovoltaic; Technology Status, Challenges, and Promise," NREL, NREL2012.

[13] S. Chu and A. Majumdar, "Opportunities and challenges for a sustainable energy future," *Nature,* vol. 488, pp. 294-303, 2012/08/16/ 2012.

[14] E. P. I. Association, "Solar Photovoltaic Electricity Empowering The World," GreenPeace, Green Peace 2011.

[15] A. Einstein, "Über einen die Erzeugung und Verwandlung des Lichtes betreffenden heuristischen Gesichtspunkt [AdP 17, 132 (1905)]," *Annalen der Physik,* vol. 14, pp. 164-181, 2005/02/23/ 2005.

[16] R. Williams, "Becquerel Photovoltaic Effect in Binary Compounds," *Journal of Chemical Physics,* vol. 32, pp. 1505-1514, 1960/05/01/ 1960.

[17] J. Singh, *Electronic and Optoelectronic Properties of Semiconductor Structures*, 1 edition ed. Cambridge: Cambridge University Press, 2007.

[18] R. F. Pierret, *Semiconductor Device Fundamentals*, 2nd edition ed. Reading, Mass: Addison Wesley, 1996.

[19] G. Committee, "Tables for Reference Solar Spectral Irradiances: Direct Normal and Hemispherical on 37 Tilted Surface," ASTM International2012 2012.

[20] J. Nelson, *The Physics of Solar Cells*: PUBLISHED BY IMPERIAL COLLEGE PRESS AND DISTRIBUTED BY WORLD SCIENTIFIC PUBLISHING CO., 2003.

[21] N. J. Tao, "Electron transport in molecular junctions," *Nature Nanotechnology,* vol. 1, pp. 173-181, 2006/12// 2006.

[22] C. Joachim, J. K. Gimzewski, and A. Aviram, "Electronics using hybrid-molecular and mono-molecular devices," *Nature,* vol. 408, pp. 541-548, 2000/11/30/ 2000.

[23] L. Lafferentz, F. Ample, H. Yu, S. Hecht, C. Joachim, and L. Grill, "Conductance of a Single Conjugated Polymer as a Continuous Function of Its Length," *Science,* vol. 323, pp. 1193-1197, 2009/02/27/ 2009.

[24] G. Cuniberti, G. Fagas, and K. Richter, "Introducing Molecular Electronics: A Brief Overview," in *Introducing Molecular Electronics*, G. Cuniberti, K. Richter, and G. Fagas, Eds., ed: Springer Berlin Heidelberg, 2005, pp. 1-10.

[25] M. Faraday, *On New Compounds of Carbon and Hydrogen, and on Certain Other Products Obtained during the Decomposition of Oil by Heat*: Royal Society of London, 1825.

[26] R. Eisberg and R. Resnick, *Quantum Physics of Atoms, Molecules, Solids, Nuclei, and Particles*, 2 edition ed. New York: Wiley, 1985.

[27] T. Engel and P. Reid, *Physical Chemistry*, 3 edition ed. Boston: Prentice Hall, 2012.

[28] A. D. McNaught and Iupac, *Compendium of Chemical Terminology - IUPAC Recommendations*, 2 Sub edition ed. Oxford England ; Malden, MA, USA: Blackwell Science Inc.

[29] M. Schwoerer and H. C. Wolf, *Organic Molecular Solids*: Wiley, 2007.

[30] W. Tress, "Device Physics of Organic Solar Cells," 2011/12/21/ 2011.

[31] S. Brazovskii and N. Kirova, "Physical theory of excitons in conducting polymers," *Chem Soc Rev,* vol. 39, pp. 2453-65, Jul 2010.

[32] R. Hull, *Properties of Crystalline Silicon*: IET, 1999.

[33] B. Ray and M. A. Alam, "Random vs regularized OPV: Limits of performance gain of organic bulk heterojunction solar cells by morphology engineering," *Solar Energy Materials and Solar Cells,* vol. 99, pp. 204-212, 2012/04// 2012.

[34] J. D. Servaites, M. A. Ratner, and T. J. Marks, "Practical efficiency limits in organic photovoltaic cells: Functional dependence of fill factor and external quantum efficiency," *Applied Physics Letters,* vol. 95, 2009 2009.

[35] D.-H. Ko, J. R. Tumbleston, A. Gadisa, M. Aryal, Y. Liu, R. Lopez*, et al.*, "Light-trapping nano-structures in organic photovoltaic cells," *Journal of Materials Chemistry,* vol. 21, 2011 2011.

[36] R. R. Lunt, N. C. Giebink, A. A. Belak, J. B. Benziger, and S. R. Forrest, "Exciton diffusion lengths of organic semiconductor thin films measured by spectrally resolved photoluminescence quenching," *Journal of Applied Physics,* vol. 105, 2009/03/11/ 2009.

[37] T. M. Clarke and J. R. Durrant, "Charge photogeneration in organic solar cells," *Chemical reviews,* vol. 110, pp. 6736-6767, 2010/11/10/ 2010.

[38] T. Kirchartz, B. E. Pieters, K. Taretto, and U. Rau, "Mobility dependent efficiencies of organic bulk heterojunction solar cells: Surface recombination and charge transfer state distribution," *Physical Review B,* vol. 80, 2009/07/31/ 2009.

[39] D. C. M. M Gross, "Improving the performance of doped pi-conjugated polymers for use in organic light-emitting diodes," *Nature,* vol. 405, pp. 661-5, 2000 2000.

[40] M. C. Scharber, D. Mühlbacher, M. Koppe, P. Denk, C. Waldauf, A. J. Heeger*, et al.*, "Design Rules for Donors in Bulk-Heterojunction Solar Cells—Towards 10 % Energy-Conversion Efficiency," *Advanced Materials,* vol. 18, pp. 789-794, 2006/03/17/ 2006.

[41] L. J. Sherry, S.-H. Chang, G. C. Schatz, R. P. Van Duyne, B. J. Wiley, and Y. Xia, "Localized Surface Plasmon Resonance Spectroscopy of Single Silver Nanocubes," *Nano Letters,* vol. 5, pp. 2034-2038, 2005/10/01/ 2005.

[42] K. A. Willets and R. P. Van Duyne, "Localized Surface Plasmon Resonance Spectroscopy and Sensing," *Annual Review of Physical Chemistry,* vol. 58, pp. 267-297, 2007 2007.

[43] J. M. Luther, P. K. Jain, T. Ewers, and A. P. Alivisatos, "Localized surface plasmon resonances arising from free carriers in doped quantum dots," *Nature Materials,* vol. 10, pp. 361-366, 2011/05// 2011.

[44] E. Petryayeva and U. J. Krull, "Localized surface plasmon resonance: Nanostructures, bioassays and biosensing—A review," *Analytica Chimica Acta,* vol. 706, pp. 8-24, 2011/11/07/ 2011.

[45] G. Mie, "Contributions to the optics of turbid media, particularly of colloidal metal solutions," *Contributions to the optics of turbid media, particularly of colloidal metal solutions Transl. into ENGLISH from Ann. Phys. (Leipzig), v. 25, no. 3, 1908 p 377-445,* vol. -1, pp. 377-445, 1976/02// 1976.

[46] H. Horvath, "Gustav Mie and the scattering and absorption of light by particles: Historic developments and basics," *Journal of Quantitative Spectroscopy and Radiative Transfer,* vol. 110, pp. 787-799, 2009/07// 2009.

[47] A. Kirkeminde, M. Retsch, Q. Wang, G. Xu, R. Hui, J. Wu*, et al.*, "Surface-passivated plasmonic nano-pyramids for bulk heterojunction solar cell photocurrent enhancement," *Nanoscale,* vol. 4, pp. 4421-4425, 2012 2012.

[48] L.-M. Chen, Z. Hong, G. Li, and Y. Yang, "Recent Progress in Polymer Solar Cells: Manipulation of Polymer:Fullerene Morphology and the Formation of Efficient Inverted Polymer Solar Cells," *Advanced Materials,* vol. 21, pp. 1434-1449, 2009/04/20/ 2009.

[49] C.-H. Chou, W. L. Kwan, Z. Hong, L.-M. Chen, and Y. Yang, "A Metal-Oxide Interconnection Layer for Polymer Tandem Solar Cells with an Inverted Architecture," *Advanced Materials,* vol. 23, pp. 1282-1286, 2011/03/11/ 2011.

[50] X. Li, W. C. H. Choy, L. Huo, F. Xie, W. E. I. Sha, B. Ding*, et al.*, "Dual Plasmonic Nanostructures for High Performance Inverted Organic Solar Cells," *Advanced Materials,* vol. 24, pp. 3046-3052, 2012/06/12/ 2012.

[51] Z. Hu, J. Zhang, Z. Hao, and Y. Zhao, "Influence of doped PEDOT:PSS on the performance of polymer solar cells," *Solar Energy Materials and Solar Cells,* vol. 95, pp. 2763-2767, 2011/10// 2011.

[52] W. Zhang, B. Zhao, Z. He, X. Zhao, H. Wang, S. Yang*, et al.*, "High-efficiency ITO-free polymer solar cells using highly conductive PEDOT:PSS/surfactant bilayer transparent anodes," *Energy & Environmental Science,* vol. 6, 2013 2013.

[53] M. Vosgueritchian, D. J. Lipomi, and Z. Bao, "Highly Conductive and Transparent PEDOT:PSS Films with a Fluorosurfactant for Stretchable and Flexible Transparent Electrodes," *Advanced Functional Materials,* vol. 22, pp. 421-428, 2012/01/25/ 2012.

[54] Y. Xia, K. Sun, and J. Ouyang, "Solution-Processed Metallic Conducting Polymer Films as Transparent Electrode of Optoelectronic Devices," *Advanced Materials,* vol. 24, pp. 2436-2440, 2012/05/08/ 2012.

[55] B. Friedel, T. J. K. Brenner, C. R. McNeill, U. Steiner, and N. C. Greenham, "Influence of solution heating on the properties of PEDOT:PSS colloidal solutions and impact on the device performance of polymer solar cells," *Organic Electronics,* vol. 12, pp. 1736-1745, 2011/10// 2011.

[56] B. Zimmermann, U. Würfel, and M. Niggemann, "Longterm stability of efficient inverted P3HT:PCBM solar cells," *Solar Energy Materials and Solar Cells,* vol. 93, pp. 491-496, 2009/04// 2009.

[57] H. M. Stec, R. J. Williams, T. S. Jones, and R. A. Hatton, "Ultrathin Transparent Au Electrodes for Organic Photovoltaics Fabricated Using a Mixed Mono-Molecular Nucleation Layer," *Advanced Functional Materials,* vol. 21, pp. 1709-1716, 2011/05/10/ 2011.

[58] L. E. Hennemann, A. Kolloch, A. Kern, J. Mihaljevic, J. Boneberg, P. Leiderer*, et al.*, "Assessing the plasmonics of gold nano-triangles with higher order laser modes," *Beilstein Journal of Nanotechnology,* vol. 3, pp. 674-683, 2012/10/04/ 2012.

[59] S. Cook, R. Katoh, and A. Furube, "Ultrafast Studies of Charge Generation in PCBM:P3HT Blend Films following Excitation of the Fullerene PCBM," *The Journal of Physical Chemistry C,* vol. 113, pp. 2547-2552, 2009/02/12/ 2009.

[60] H. Chen, X. Kou, Z. Yang, W. Ni, and J. Wang, "Shape- and size-dependent refractive index sensitivity of gold nanoparticles," *Langmuir,* vol. 24, pp. 5233-7, May 20 2008.

[61] S. Dengler, C. Kübel, A. Schwenke, G. Ritt, and B. Eberle, "Near- and off-resonant optical limiting properties of gold–silver alloy nanoparticles for intense nanosecond laser pulses," *Journal of Optics,* vol. 14, 2012/07/01/ 2012.

[62] Y. Zhou, C. Fuentes-Hernandez, J. Shim, J. Meyer, A. J. Giordano, H. Li*, et al.*, "A Universal Method to Produce Low–Work Function Electrodes for Organic Electronics," *Science,* vol. 336, pp. 327-332, 2012/04/20/ 2012.

[63] Z. He, C. Zhong, X. Huang, W.-Y. Wong, H. Wu, L. Chen*, et al.*, "Simultaneous Enhancement of Open-Circuit Voltage, Short-Circuit Current Density, and Fill Factor in Polymer Solar Cells," *Advanced Materials,* vol. 23, pp. 4636-4643, 2011/10/25/ 2011.

[64] D.-w. Choi, S.-J. Kim, J. H. Lee, K.-B. Chung, and J.-S. Park, "A study of thin film encapsulation on polymer substrate using low temperature hybrid ZnO/Al2O3 layers atomic layer deposition," *Current Applied Physics,* vol. 12, Supplement 2, pp. S19-S23, 2012/09// 2012.

[65] C. Lungenschmied, G. Dennler, H. Neugebauer, S. N. Sariciftci, M. Glatthaar, T. Meyer*, et al.*, "Flexible, long-lived, large-area, organic solar cells," *Solar Energy Materials and Solar Cells,* vol. 91, pp. 379-384, 2007/03/06/ 2007.

[66] J. Granstrom, J. S. Swensen, J. S. Moon, G. Rowell, J. Yuen, and A. J. Heeger, "Encapsulation of organic light-emitting devices using a perfluorinated polymer," *Applied Physics Letters,* vol. 93, 2008/11/12/ 2008.